

Water megamaser emission in hard X-ray selected AGN

F. Panessa¹, P. Castangia², A. Malizia³, L. Bassani³, A. Tarchi², A. Bazzano¹, and P. Ubertini¹

¹ Istituto di Astrofisica e Planetologia Spaziali di Roma (IAPS-INAF), Via del Fosso del Cavaliere 100, 00133 Roma, Italy
e-mail: francesca.panessa@inaf.it

² Osservatorio Astronomico di Cagliari (OAC-INAF), Via della Scienza 5, 09047 Selargius (CA), Italy

³ Osservatorio di Astrofisica e Scienza dello Spazio di Bologna (OAS-INAF), Via P. Gobetti 101, 40129 Bologna, Italy

Received 23 December 2019 / Accepted 12 June 2020

ABSTRACT

Context. Water megamaser emission at 22 GHz has proven to be a powerful tool for astrophysical studies of active galactic nuclei (AGN) because it allows an accurate determination of the mass of the central black hole and of the accretion disc geometry and dynamics. However, after searches among thousands of galaxies, only about 200 of them have shown such spectroscopic features, most of them of uncertain classification. In addition, the physical and geometrical conditions under which a maser activates are still unknown.

Aims. We characterize the occurrence of water maser emission in an unbiased sample of AGN by investigating the relation with the X-ray properties and the possible favourable geometry that is required to detect water maser.

Methods. We searched for 22 GHz maser emission in a hard X-ray selected sample of AGN, taken from the INTEGRAL/IBIS survey above 20 keV. Only half of the 380 sources in the sample have water maser data. We also considered a volume-limited sub-sample of 87 sources, for which we obtained new observations with the Green Bank and Effelsberg telescopes (for 35 sources). We detected one new maser and increased its radio coverage to 75%.

Results. The detection rate of water maser emission in the total sample is $15\pm 3\%$. This fraction increases to $19\pm 5\%$ for the complete sub-sample, especially when we consider type 2 ($22\pm 5\%$ and $31\pm 10\%$ for the total and complete samples, respectively) and Compton-thick AGN ($56\pm 18\%$ and $50\pm 35\%$ for the total and complete samples, respectively). No correlation is found between water maser and X-ray luminosity. We note that all types of masers (disc and jet) are associated with hard X-ray selected AGN.

Conclusions. These results demonstrate that the hard X-ray selection may significantly enhance the maser detection efficiency over comparably large optical or infrared surveys. A possible decline in detection fraction with increasing luminosity might suggest that an extremely luminous nuclear environment does not favour maser emission. The large fraction of CT AGN with water maser emission could be explained in terms of geometrical effects. The maser medium would then be the very edge-on portion of the obscuring medium.

Key words. galaxies: active — galaxies: Seyfert — masers — X-rays: galaxies — gamma-rays: galaxies — surveys

1. Introduction

One of the most common maser emission lines arises from the water rotational transition levels 6_{16} and 5_{23} , which emit at 22 GHz in the radio domain. Extra-galactic water masers trace warm ($T_{kin} > 300$ K) and dense ($10^7 \text{ cm}^{-3} < n(\text{H}_2) < 10^{11} \text{ cm}^{-3}$) gas (Elitzur 1992; Neufeld et al. 1994). Water maser sources with an isotropic luminosity below $10 L_{\odot}$ are defined as kilo-masers, while at higher luminosity, they are defined as mega-masers. The latter are generally associated with the activity of active galactic nuclei (AGN), while kilo-masers are more commonly related to star formation in the host galaxy (this distinction should, however, be used with caution, see Sect. 4.2 in Tarchi et al. (2011) and this work Sect.3).

The activity of water maser emission in AGN has been associated with three main different phenomena (see e.g. Lo 2005; Tarchi 2012). A typical triple-peak system of lines is associated with an accretion disc emission (one systemic, one blueshifted, and one redshifted), whose geometry and rotation velocities can be traced by very long baseline interferometry (VLBI, e.g. Miyoshi et al. 1995; Greenhill et al. 2003). On the other hand, the interaction between the radio jet and the molecular clouds or the overlap along the line of sight between the molecular cloud and radio continuum emission from the jet might produce wa-

ter maser emission in the form of a single broad redshifted (or blueshifted) line (e.g. Gallimore et al. 2001; 1996; Henkel et al. 2005). Jet velocity and density were estimated in a reverberation mapping analysis (Peck et al. 2003). Finally, in the case of the Circinus galaxy, the water maser emission has shown two different dynamic components in VLBI mapping: one associated with a warped disc, and another with a wide-angle nuclear outflow (Greenhill et al. 2003). Outflowing maser components have also been detected in NGC 3079 (Kondratko et al. 2005).

So far, more than 4000 galaxies have been searched for water maser emission, and detections have been obtained in about 160 of them (180 when starburst galaxies are also included; Megamaser Cosmology Project, MCP¹), the majority are radio-quiet AGN in the local Universe ($z \leq 0.05$), classified as Seyfert 2 or low-ionisation nuclear emission-line regions (LINERs). The overall detection rate in large maser surveys is rather low (e.g. Braatz et al. 1997; Greenhill et al. 2003; Van den Bosch et al. 2016) and is about 3% for sources observed within the MCP, which mainly targets galaxies selected from large optical surveys, such as SDSS, 6dF, and 2MRS (Braatz et al. 2015; see also Greenhill et al. 2003; Zhu et al. 2011). Hagiwara et al. (2002;

¹ <https://safe.nrao.edu/wiki/bin/view/Main/MegamaserCosmologyProject>

2003) selected their targets based on the ratio of radio continuum to IR (60 μ and 100 μ) flux densities from IRAS galaxies and obtained a slightly higher detection rate of 8%. Henkel et al. (2005) later confirmed that the far-IR selection favours maser detection. These authors found a detection rate of 22% in a sample of northern galaxies with an IRAS point source flux density at 100 micron greater than 50 mJy. More recently, Kuo et al. (2018) found that galaxies with water maser detection tend to be associated with strong IR emission, as observed by the WISE telescope, thus offering a way to boost the detection rate to 6–15%. It has also been suggested that radio emission is a suitable indicator for water maser emission (Zhang et al. 2012, 2017), and the radio luminosities of maser galaxies indeed tend to be higher by a factor of 2–3 than those in non-masing galaxies (Liu et al. 2017).

Finally, the fraction of water maser detection has been found to be around 26% in a sample of Seyfert galaxies located within 20 Mpc. This suggests that an observational bias in terms of distance is also likely (Panessa & Giroletti 2013).

The maser detection efficiency might be improved if high-luminosity objects were selected (Zhu et al. 2011). However, the largest fraction of nuclear water masers seems to be associated with type 2 Seyfert galaxies and a high level of X-ray obscuration (Greenhill et al. 2008), in particular to Compton-thick AGN (CT AGN are defined as sources with an X-ray obscuration of $N_H > 10^{24}$ cm $^{-2}$. This is the inverse of the Thomson cross section), (Greenhill et al. 2003; Castangia et al. 2019). This is in line with the predictions of unified models for AGN (Antonucci, & Miller 1985), in which an obscuring torus that is aligned with the accretion disc at larger scales is responsible for the observed obscuration and for the optical classification of the AGN (see Padovani et al. 2017 for a review). Interestingly, the fraction of CT obscuration increases in disc masers (Greenhill et al. 2008), as was confirmed by X-ray studies of known disc masers (Castangia et al. 2013; Masini et al. 2016). In order to be detected, maser discs should be observed nearly edge-on to the observer line of sight. This suggests that the X-ray obscuring material and the maser disc are connected. Masers might indeed trace molecular material associated with the torus or the outer regions of the accretion disc. All the different proposed geometries (Elitzur, & Shlosman 2006; Tilak et al. 2008; Masini et al. 2016) take into account that long path lengths are needed to produce maser amplification, therefore the observer line of sight has to be close to an edge-on orientation. In this respect, warped discs, as have been observed in the prototype NGC 4258 (Herrnstein et al. 1997), increase the probability that the line of sight is intercepted. The disc has to be warped to be directly illuminated by the X-ray radiation from the central engine, as envisaged by the theory of maser production (Neufeld et al. 1994). More recently, Darling (2017) discussed the interesting possibility that some water maser sources might be detected that are associated with inclined accretion discs (more than 10 degrees from edge-on) and orbit massive black holes. The detection would be made by the lensing or deflection of in-going systemic maser features.

Even though objects with higher X-ray luminosity and/or higher column density more likely host masers, there is no large sample of AGN with X-ray data available so far for a target selection, nor has a similar type of study been performed on a statistically meaningful basis. This work aims at filling this gap and at providing some useful means to improve the maser detection efficiency by pre-selecting targets from hard X-ray surveys, which so far are the least biased in terms of intrinsic AGN absorption.

Throughout this paper we assume a flat Λ cold dark matter cosmology with $(\Omega_M, \Omega_\Lambda) = (0.3, 0.7)$ and a Hubble constant of 70 km s $^{-1}$ Mpc $^{-1}$ (Jarosik et al. 2011).

2. Sample definition

We concentrate on a sample of active galaxies selected in hard X-rays (or soft gamma-ray band, defined above 20 keV). This waveband provides a very efficient way to find nearby AGN (unabsorbed and absorbed) because it is transparent to obscured regions or objects, that is, those that might be missed at other frequencies such as optical, UV, and even X-rays below 10 keV. Since 2002, the hard X-ray sky is being surveyed by INTEGRAL/IBIS (Ubertini et al. 2003) and subsequently by Swift/BAT (Gehrels et al. 2004) at energies greater than ~ 20 keV; various all-sky catalogues have been released based on the data collected by these two satellites (see e.g. Bird et al. 2016; Baumgartner et al. 2013 and Oh et al. 2018). These catalogues contain large fractions of active galaxies, about 40% of the INTEGRAL/IBIS and up to 70% of the Swift/BAT sources. These two samples together provide the most extensive list of hard X-ray selected active galaxies known to date.

For the purpose of this work, we used the large sample of AGN extracted from INTEGRAL/IBIS data. For comparison purposes alone, we consulted two samples extracted from Swift/BAT surveys (the 9-month and 70-month samples).

For INTEGRAL, we considered the sample of 272 AGN discussed by Malizia et al. (2012), to which we added 108 sources that have been discovered or identified with active galaxies afterwards (Malizia et al. 2016). This set of 380 hard X-ray selected AGN represents our reference catalogue and was used as the main input for this work. The main advantage of this sample is that it is fully characterised in terms of optical class, redshift, and X-ray properties, including information on the X-ray and hard X-ray fluxes and X-ray column density. Unfortunately, due to the INTEGRAL observing strategy, this sample is not complete or uniform, and to overcome this limitation, we considered a subset of AGN (all included in the sample of 380 objects) that instead represent a complete sample. This sample, which is fully discussed in Malizia et al. (2009), consists of 87 galaxies that are detected in the 20–40 keV band and listed in the third IBIS survey (Bird et al. 2007). We note that one source, IGR J03184-0014, is not considered here as it was never again detected in subsequent INTEGRAL surveys. To investigate maser emission in the entire sample of 380 AGN, we consulted the catalogues maintained on the website of the MCP, which is the largest and most comprehensive catalogue of all galaxies that have been surveyed for water maser emission at 22 GHz (Reid et al. 2009; Braatz et al. 2010). The catalogue has been updated on a regular basis to include all of the new observations and associated findings. To integrate the MCP data and to cover our sample as far as possible, we also searched the literature for reports of water maser observations or detections. Finally, 35 galaxies belonging to the complete sample were observed for the first time in search for 22 GHz water maser emission using the Effelsberg telescope and the Green Bank Telescope (GBT). We discovered new maser (Sect. 3). Table 1A lists all 380 INTEGRAL/IBIS AGN (see Appendix A for a detailed description).

In Fig. 1 we plot the hard X-ray luminosity as a function of redshift (in logarithmic scale) for the total sample (left panel) and the complete sample (right panel). We divide the AGN into those that are not observed at 22 GHz, those that are observed, and those that are detected. This figure clearly shows that objects at high redshift and high hard X-ray luminosity are almost not

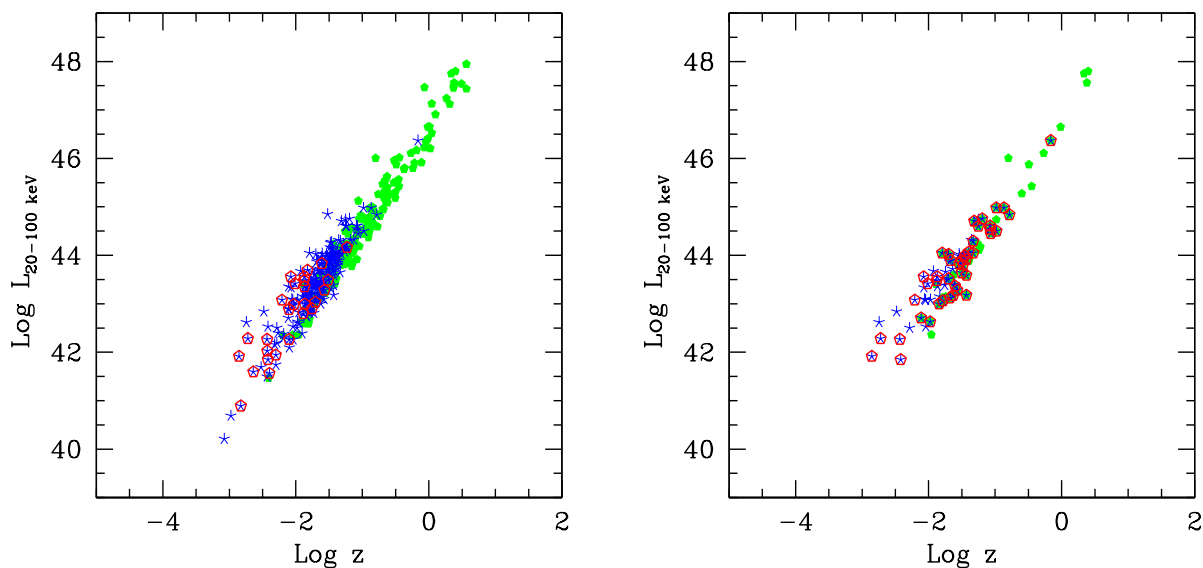


Fig. 1: Hard X-ray luminosity (20–100 keV) vs. redshift logarithm. Green dots represent the sources that are not observed at 22 GHz, blue stars are observed sources, and red open polygons are detected sources. Left panel: Total sample of 380 AGN. Right panel: Complete sub-sample of 87 AGN.

covered by maser observations. Furthermore, we compared the redshift and luminosity distributions of the total and complete samples in order to confirm whether they belong to the same parent population (null hypothesis). A Kolmogorov–Smirnov (KS) test results in p-values of 0.10 (z) and 0.59 ($L_{20-100\text{keV}}$), therefore the null hypothesis cannot be rejected at the 1% level. This suggests that the two samples might be considered statistically equivalent, that is, likely affected by similar biases. We performed the same test and only considered the observed sources in the two samples. The KS test results in p-values of 0.75 (z) and 0.41 ($L_{20-100\text{keV}}$), and again, the null hypothesis cannot be rejected at the 1% level. We conclude that the total and complete samples of hard X-ray selected AGN with water maser observations are representative of the local Universe and thus constitute an ideal set in which to study water maser occurrence in nearby super-massive black holes.

3. Observations, data reduction, and results

3.1. GBT observations

We observed the $6_{16}-5_{23}$ transition of ortho- H_2O (rest frequency 22.23508 GHz) towards 28 galaxies of the complete INTEGRAL sample with the GBT between March 2010 and January 2011 (projects AGBT10A-042 and AGBT10C-012). We used the 18–22 GHz dual-beam receiver in nod mode and kept one of the two beams alternately on-source during integration. The GBT spectrometer was configured with two 200 MHz IFs offset by 180 MHz for a total coverage of 380 MHz (corresponding to 5100 km s^{-1} at 22 GHz). The first spectral window was centred at the frequency corresponding to the recessional velocity of each galaxy, and the second was offset to the red. This setup yielded a channel spacing of 24 kHz ($\sim 0.3 \text{ km s}^{-1}$ at 22 GHz) per spectral

window. We reduced and analysed the data with `GBTIDL`². Flux calibration was performed using standard routines and applying the default zenith opacity and gain curve. The estimated uncertainty of the absolute flux calibration is $\sim 20\%$ (for details, see the guide for calibrating GBT spectral line data using `GBTIDL`³).

3.2. Effelsberg observations

On April 15 and 16, 2011, we used the Effelsberg 100 m telescope to search for 22 GHz water maser emission in seven galaxies of the complete INTEGRAL sample (3C 111, IC 4329A, IGR J16482, 2E 1739, IGR J17513, IGR J21247, and BLLAC). We employed the 1.3 cm primary focus (PFK) receiver (17.9–26.2 GHz) with a fast Fourier transform (FFT) spectrometer encompassing 100 MHz and 16384 channels. This setup yielded a channel spacing of 6.1 kHz, corresponding to 0.08 km s^{-1} at 22.2 GHz. We observed in position-switching mode, with the off-position offset by 15 arcminutes in right ascension. Signals from individual on- and off-source positions were integrated for 120 s each. The data were reduced using the GILDAS software package (e.g. Guilloateau & Lucas 2000). To convert the measured signal from counts into antenna temperature, we used the tabulated values of the noise diode in K. We then applied the normalised gain curve and multiplied by the standard value of the sensitivity⁴. The uncertainty of this flux calibration was derived by applying the same procedure to continuum-pointing scans of NGC 7027, and it is estimated to be $\sim 30\%$.

² <http://gbitidl.nrao.edu>

³ https://www.gb.nrao.edu/GBT/DA/gbitidl/gbitidl_calibration.pdf

⁴ Calibration information for the 1.3 cm PFK receiver is reported in the Effelsberg Wiki page <https://eff100mwiki.mpi-fr-bonn.mpg.de/doku.php>.

3.3. Results

During our survey, a new water maser was detected with the GBT in the narrow line Seyfert 1 (NLSy1) galaxy IGR J16385-2057 on March 28, 2010. This discovery, and hence the line profile and the characteristics of the water maser emission, has been anticipated in a previous paper by our team, which was focused on water maser emission in NLSy1 galaxies (Tarchi et al. 2011). Here, we report in Table 1A the isotropic line luminosity. In Table 1A we also list the 1σ rms and the upper limit on $L_{\text{H}_2\text{O}}$ for the remaining 33 targets, with the exception of 3C 273. The strong radio continuum emission of the blazar jet ($S_{22}=27\text{-}43$ Jy, e.g. Gear et al. 1994) affects the GBT spectral baseline, which is visible as strong ripples. These prevented us from estimating a reliable rms for this source and from assessing the presence (or absence) of an emission line. As a consequence, 3C 273 is labelled ‘not observed’ in Table 1A.

Although we were unable to reach the full coverage of the complete sample at 22 GHz, we were able to increase the number of sources with water maser observations from the initial 31 with data in the literature to 65 (34 from our own survey). This increases the coverage from 36% to 75%.

Within the sample of 34 objects that were observed for the first time, the maser detection rate is rather low (1 of 34, or <6%), but this is likely due to the optical classification of the observed sources: most objects (26) belong to the type 1 classification, and only 8 sources are of type 2. The one detected maser belongs to the class of NLSy1, which indeed seems to have a high probability of hosting maser emission (Tarchi et al. 2011). In this respect, the fraction of detected maser within these newly observed AGN is consistent with the average fraction of detected masers in type 1 objects (see next Sect.). We also searched for further biases that might be introduced by the lack of full radio observation coverage of the complete sample in addition to the known bias against high redshift and luminosity. We compared the distribution of X-ray absorption and position in the sky of the observed and unobserved sources. The test did not reveal significant differences between the two sub-samples in terms of absorption (KS p -value=0.09) or position in the sky (KS p -value=0.23).

4. Maser fraction at high energies

Out of 380 objects in the total sample, 193 have been observed at 22 GHz. This is only $51\pm 4\%$ of the sample. In the complete sample, 65 out of 87 objects were observed at this frequency. This provides a coverage of almost 75%.

Considering the total set of INTEGRAL AGN reported in Table 1A, we found that out of 193 galaxies observed at 22 GHz, 29 have been reported as maser sources; this represents a detection rate of $15\pm 3\%$. Errors on the fractions were calculated as $\sqrt{N_M}/N_O$, where N_M is the number of detected maser sources and N_O is the number of observed sources. To take unobserved sources into account and thus provide a range of values for the entire sample, we can take two extreme approaches and assume that if pointed, all not yet observed INTEGRAL AGN are found to be undetected at 22 GHz (lower range), or alternatively, that all are detected (upper range). Under these conditions, we find that the detection rate for the whole sample ranges from 8 to 57%. This a rather wide range that nevertheless tells us that the detection rate in the worst case is higher than is generally obtained using large samples of optically selected galaxies (Sect. 1). Out of 29 objects with maser detection, the 22 GHz luminosity is below $10 L_\odot$ for 6 objects (i.e. Mkn 3, NGC 4051, NGC 4151, Mkn 766, Cen A, and NGC 6300) and they therefore qualify to

be kilo-maser objects. However, some of these sources were imaged at high resolution and their maser emission was found to be located within the nuclear region of the host galaxies. Therefore, given that all our sources are hard X-ray emitters and can confidently be associated with an accreting supermassive black hole, we confirm that kilo-maser emission may not only be associated with star formation, but also with AGN activity, as has been suggested by Tarchi et al. 2011.

When we instead consider the complete sample of INTEGRAL sources that is highlighted in Table 1A, 65 AGN are observed at 22 GHz, of which 12 are detected and only 22 are unobserved. In this case, the detection rate is $19\pm 5\%$ and the range of possible values lies between 14 and 39%.

Because water maser emitters show a preference to be found in type 2 AGN, we also restricted our analysis to Seyfert 2 galaxies alone (including intermediate types 1.8-1.9), which are present either in the total or in the complete INTEGRAL samples. In this case, we find that the sample coverage was 68% (103 AGN observed, 23 detected, and 60 unobserved) and 88% (29 AGN observed, 9 detected, and 5 unobserved) for the total and complete sample, respectively: we therefore estimate a detection rate of $22\pm 5\%$ (range values from 14 to 51%) and $31\pm 10\%$ (range values from 27 to 41%) for each of these two samples.

These fractions are even more remarkable when they are compared to those of Seyfert 1 (in this case, also including intermediate types 1.2-1.5): 74 objects have water maser observations of the type 1 AGN, but only two (NGC 4151 and NGC 3783) have been detected. This implies a detection fraction of about 3%, which is similar to what we found within the MCP (see also König et al. 2012). Interestingly, the detection rate of NLSy1, which are also broad-line AGN but have peculiar characteristics at multi-frequencies with respect to standard broad line AGN (see e.g. Panessa et al. 2011), is comparable to those of Seyfert 2. Our sample includes 9 NLSy1 with 22 GHz measurements and 3 water maser detections (NGC 4051, Mkn 766, and IGR J16385-2057), which implies rates close to 30%. This confirms previous results obtained by Tarchi et al. (2011) in a dedicated study of this type of AGN, in which the authors suggested an outflow origin for water maser emission. Mathur (2000) proposed that NLSy1 sources might be young AGN residing in rejuvenated galaxies; alternatively, their peculiarities might be explained in terms of an orientation effect that is caused by the pole-on observation of their broad-line region (Decarli et al. 2008). The link of these two interpretations to the maser phenomenon in these peculiar objects is still unclear, but confirmation of high detection rates in NLSy1 indicates that this question requires more in-depth studies.

To consolidate our overall results, we also compared the above rates with those obtained from the 70-month (Baumgartner et al. 2013) and 9-month (Tueller et al. 2008) Swift/BAT samples. These two samples were selected to be almost comparable in size with the INTEGRAL total and complete sub-samples.

The 70-month BAT survey provides the list of all objects detected by the instrument during the first 6.8 years of the Swift mission and covers 90% of the sky at a sensitivity level of 1.3×10^{-11} ergs $\text{s}^{-1}\text{cm}^{-2}$ in the 14–195 keV band. The sample contains a large fraction of unclassified sources that may turn out to be AGN after proper follow-up work; thus our search for maser detection provides only an indication of the level of maser occurrence in this large BAT sample. To search for water maser emission in this set of hard X-ray selected AGN, we were helped by three high-school students during a stage performed at OAS/INAF in Bologna in 2016. As for the INTE-

Table 1: Summary of the detection fractions for different samples and sub-samples.

Sample (Number of AGN observed at 22GHz)	DF (Detection fraction in %)	DF (Detection fraction in %) range
INTEGRAL total (285)	15.0±2.8	7.6-57.0
INTEGRAL complete (65)	18.5±5.3	13.8-39.0
INTEGRAL Sey1.8-2 total (103)	22.0±4.7	13.5-51.0
INTEGRAL Sey1.8-2 complete (29)	31±10	27-41
INTEGRAL Sey1-1.5 total (74)	2.7±1.9	1.4-51.0
INTEGRAL NLSy1 total (9)	33±19	20-60
Swift/BAT 70M (285)	12.6±2.1	-
Swift/BAT 9M (114)	14.9±3.6	11-37
Swift/BAT 9M Sey2 (51)	25.5±7.0	20-41
DS optical (89)	23.6±5.1	-
DS optical Sey2(71)	26.8±6.1	-

GRAL sample, we searched the available archives, such as the MCP and the literature, for reports of water maser observations and detections for all 822 AGN reported in the BAT survey. Altogether, we found that only 285 objects of this sample (only 35%) have been observed at 22 GHz and 36 objects have been detected. The detection fraction is therefore about 13±2%, which perfectly agrees with our INTEGRAL results. Most of the detections overlap the INTEGRAL detections; the additional sources are NGC 235A, UGC 3157, VII Zw 073, NGC 3393, CGCG 164-019, MKN 78, UGC 5101, and M 82 considering that IGR J16385-2057 and NGC 6926 were only detected by INTEGRAL. We note that in the case of M 82, the emission above 10 keV is dominated by a few ultra-luminous X-ray sources (ULXs) with a minor contribution from lower luminosity X-ray binaries (Vulic et al. 2018) and can therefore not be attributed to AGN activity.

The Swift/BAT 9-month catalogue contains only 154 sources (all of which are identified and optically classified as AGN) and covers 74% of the sky (only the sky above ±15 degrees in latitude was considered to avoid contamination by galactic objects) at a flux threshold of 5×10^{-11} ergs s⁻¹cm⁻² in the 14–195 keV band. In this catalogue, 114 objects have been observed at 22 GHz and 17 are detected (listed in Table 2A). Only 40 AGN have no observational coverage at the waveband of interest here. The detection rate is 15±4%. Applying the same exercise as for the INTEGRAL samples (i.e. assuming all unobserved sources to be either detected or undetected at 22 GHz), we estimate a possible range of values between 11 and 37%. When we restrict this to type 2 AGN alone, 51 of 65 objects in this sample have been observed, and 13 objects display maser emission. This provides a detection rate close to 26±7%. In this case, the possible range of values is estimated to vary from 20 to 41%, which again fully agrees with the estimates obtained from the INTEGRAL samples.

Finally, we compared our results, in particular, those obtained for type 2 Seyferts, with the optical data set of AGN discussed by Diamond-Stanic et al. (2009). These authors have compiled a complete sample of 89 Seyfert galaxies, made of 18 type 1 (1-1.5) and 71 type 2 (1.8-2) AGN, all within a distance of 200 Mpc. The entire sample has been covered by water maser observations and is therefore a reference catalogue for this type of studies. There are 21 masers (listed in Table 3A) and 68 non-maser sources in this sample, providing a detection rate of 24±5%. When we restrict the estimate to Seyfert 2 galaxies alone, the detection rate increases only slightly to 27%, again in full agreement with the estimate provided in this work. The highest detection rate found in this sample appears to contrast with estimates obtained using other optically selected samples

of AGN (e.g. Zhu et al. (2011) quote a detection rate of almost 8% for Seyfert 2 galaxies), but this may be due to the fact that the Diamond-Stanic et al. (2009) sample is biased in favour of close-by AGN, mostly of type 2, similarly to the sample that was investigated in Panessa & Giroletti (2013).

The detection fractions for all samples considered in this work are summarised in Table 1, which clearly shows that hard X-ray catalogues provide a significant boost of the maser detection fraction with respect to large optical surveys (e.g. Zhu et al. 2011; Braatz et al. 2018): they reach values of at least 15-25%. These values are also higher than those obtained by specifically tuning the AGN selection in the IR band using different criteria and combining them, as recently proposed by Kuo et al. (2018). Furthermore, the hard X-ray selection, in addition to providing a catalogue of galaxies with a high probability of maser detection, also provides a set of sources with clear evidence of AGN activity and therefore negligible or null contamination from star-forming objects.

5. Improving the detection probability

In Fig. 2 we plot the water maser detection rate in our total sample and in the complete sub-sample as a function of redshift (left panel), X-ray nuclear absorption (middle panel), and 20–100 keV hard X-ray luminosity (right panel). For the distribution of the water maser fraction as a function of redshift and column density, objects were grouped so that about the same number of observed sources is shown in each bin. For the distribution in luminosity, this was more difficult to achieve while still maintaining a reasonable number of bins, but the uncertainty related to this choice is reflected in the error associated with each bin.

It is evident that water maser detection decreases as a function of redshift from about 40-60% at low redshifts to a few percent at higher distances (above $z=0.015$), in agreement with the distance bias discussed in Sects. 2 and 3. In contrast, the detection fraction increases for higher X-ray column densities from a few percent to 25-40% at a threshold of 10^{23} cm⁻² and reaches 56±18% above the Compton-thick regime in the case of the total sample (50±35 for the complete sample). This again confirms that the water maser detection is favoured among heavily absorbed AGN. The hard X-ray luminosity also appears to play a role, although in these cases, the error bars are larger and the scarce observations of highly luminous sources may affect this result: a decline in detection fraction is seen from low to high luminosities, which may be an indication that an extremely luminous nuclear environment does not favour maser emission. As discussed in Castangia et al. (2013 and references therein), for high nuclear bolometric luminosities or environ-

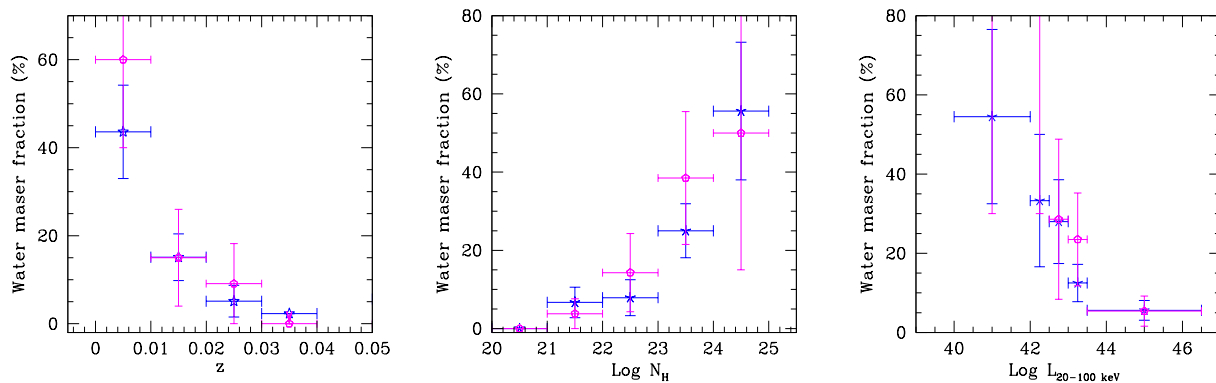


Fig. 2: Fraction of detected water maser emission vs. redshift limited to $z < 0.04$, X-ray column density in cm^{-2} (central panel), and 20–100 keV luminosity in $\text{ergs s}^{-1} \text{cm}^{-2}$ (right panel). Blue starred points represent the total sample, and magenta polygons show the complete sub-sample.

ments that are particularly heavily exposed to strong X-ray radiation, H_2O maser emission at sub-parsec distances from the nucleus of the galaxy may be hampered because the ISM is mostly atomic and/or the dust grains (where water is thought to be often formed) are destroyed. While maser emission can still be produced at larger distances, the innermost (hundredths of parsecs) masing action would be prevented if this scenario is correct. In addition, an increased bolometric luminosity might decrease the maser emissivity by reducing the difference between gas and dust temperatures (Kuo et al. 2018), on which the volume rate of maser photon production significantly depends (Gray et al. 2016).

The fractions for the total and the complete sub-samples are consistent within the errors and the trends are confirmed for the two samples. However, the statistics is limited by the small number of data sets, especially for the complete sub-sample.

6. Maser type of INTEGRAL AGN

Most maser detections reported in this work have been discussed in the literature and their maser type has been analysed in previous works (see type and relative references in the notes of Table 1A). In the following and in Table 1A, we considered as disc, outflow, or jet maser sources for which the maser class is either fully assessed or just suggested on the basis of observational results; for these last objects, only follow-up, mainly interferometric VLBI, continuum, and spectral line studies can confirm a water maser association with AGN activity and maser type.

Only 6 sources in the sample of 29 maser detections (IGR J05081+1722, NGC 3081, NGC 3783, NGC 5643, NGC 6300, and ESO 103-G35) have no associated maser classification; in Appendix B we attempt to provide some indication of the possible nature of these sources and implicitly discuss their most likely maser type. Table 1A shows that the water maser classification generally refers to one, or in some cases, two components, such as a disc plus outflow or jet.

When we exclude these 6 sources from our sample of AGN with 22 GHz detection, we note that similar numbers (12-12) of objects have a disc (or evidence of disc) and a jet (or evidence of jet) water emission; outflow or evidence of outflow emission is present in 7 sources. Despite the uncertainties involved in water maser classification, it is evident from the present sample that

all types of masers are likely associated with INTEGRAL AGN and that discs masers are not necessarily the dominant type. Thus hard X-ray surveys also offer the opportunity of probing masers of different types.

Finally, we note that the maser type of all optical narrow-line AGN (including type 1 and NLSy1) is likely related to jet and/or outflow emission, and none is apparently associated with accretion discs. Type 2 AGN instead seem to display all types of water masers: out of 24 Seyfert 2 that are detected, the emission in 12 is partly or entirely associated with a disc, in 8 with a jet, and only in 3 with outflow. Maser sources associated with edge-on ($i = 90 \pm 10$ degrees, see Sect. 8) discs are most likely, and not surprisingly according to the unified model, found in type 2 AGN.

7. Maser versus non-maser INTEGRAL AGN

One main question that is still unanswered in extragalactic maser astrophysics is related to the conditions that lead to maser emission in only a fraction of AGN. It is therefore reasonable to ask whether water maser galaxies have special intrinsic properties in terms of X-ray/hard X-ray luminosities and absorption compared to apparently similar galaxies without detected maser emission.

According to theory, high-energy radiation from the central part of an AGN could heat the circumnuclear gas temperature to values suitable for maser emission (Neufeld et al. 1994); in this case, we expect a relationship between the maser luminosity and the X-ray/hard X-ray luminosities. Kondratko et al. (2006) studied a sample of 30 water maser AGN and indeed found such a relation ($L_X \propto L_{\text{H}_2\text{O}}^{0.5}$), where L_X is the unabsorbed X-ray luminosity in the 2–10 keV band; the significance of this correlation improved when the sample was limited to disc masers. However, the relation still presented a large scatter, likely due to a dependence on different parameters, such as the mass accretion rate, the ratio of X-ray to bolometric luminosity, and the well-known X-ray and maser variability (in the latter, this typically is about some dozen percent, e.g. Maloney (2002) and references therein). This relation seems to be weak or absent in more recent studies even when only disc maser sources were considered, which are the sources in which the correlation is expected to be stronger (Castangia et al. 2013).

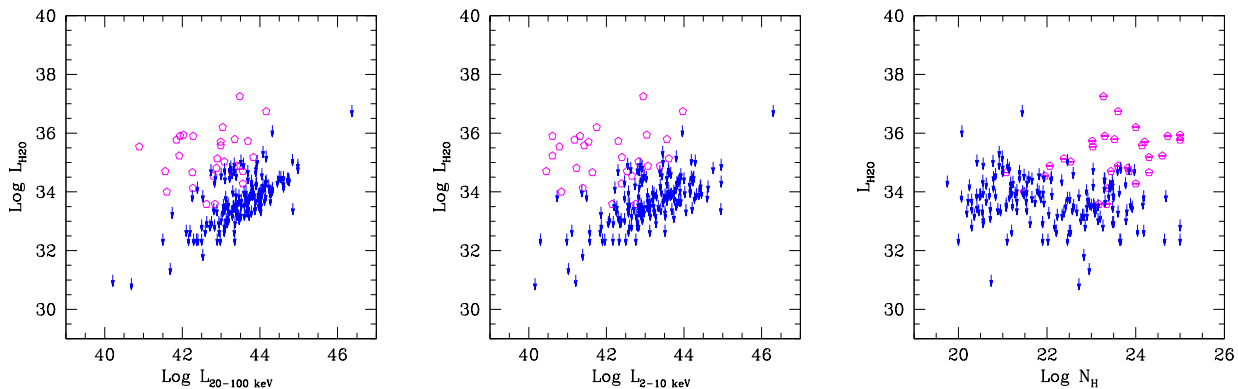


Fig. 3: Logarithmic water maser luminosity vs. 20–100 keV (left panel) and 2–10 keV logarithmic luminosities (central panel), expressed in $\text{ergs s}^{-1} \text{cm}^{-2}$. Water maser luminosity vs. the logarithmic X-ray column density in cm^{-2} (right panel). Empty magenta polygons are water maser detected sources, and blue arrows represent the upper limits to the water maser luminosity.

A more direct estimate of the AGN radiation field is provided by the hard X-ray luminosity, which is the least affected in terms of nuclear absorption; this information is available for all our objects and has never been employed before in a correlation with the maser luminosity. In Fig. 3 (left and middle panels) we therefore plot the isotropic water maser luminosity as a function of the 20–100 keV and 2–10 keV observed luminosities. When the regression analysis is only applied to the detected sources, the Spearman Rho correlation coefficients are 0.16 and 0.10, providing a two-tailed probability of 0.42 and 0.59, respectively. Therefore the association between the two variables should not be considered statistically significant. The sources of scatter as discussed in Kondratko et al. (2006) analogously apply to our relations.

Finally, we note here also that the range of hard X-ray and X-ray luminosities of detected masers cover a similar interval as non maser AGN, therefore no evident luminosity threshold could be identified as maser activator above $L_{2-10\text{keV}} \sim 10^{40} \text{ ergs s}^{-1}$. In addition, the sensitivity of 22 GHz surveys is no limit for maser detection because luminosity upper limits are also found at a factor of about 10 to 100 below detections.

As discussed by Zhang et al. (2006), a correlation between water maser luminosity and X-ray absorption (approximately $L_{\text{H}_2\text{O}} \propto N_{\text{H}}^3$) is also expected for idealised saturated maser emission (assuming no velocity gradients in the maser region). In this case, the value of the exponent is determined by the luminosity that linearly increases with the column density and the surface of the masing cone, which grows with the square of its lengths (e.g. Kylafis & Norman 1991). In Fig. 3 (right panel), we display the isotropic water maser luminosity as a function of the X-ray absorption for maser and non-maser sources. When we again consider only detected sources, the resulting Spearman Rho correlation coefficient is 0.37 with a derived two-tailed probability of 0.05, suggesting that the association between the two variables might only be marginally considered statistically significant. This again confirms that the X-ray obscuring medium is associated with the masing material.

While an interpretation based on the different maser types would be interesting, it would reduce the number of sources that are tested because variety of maser types in our sources is great. This would weaken the significance of these relations. In ad-

dition, the high complexity of the different maser components complicates the interpretation of these correlations.

8. Water masers in Compton-thick AGN

Of the 21 objects of the total sample in the CT regime, 8 have no maser detection, 10 have a maser detection, and 3 have not yet been observed. Therefore the probability is about $56 \pm 18\%$ to detect maser emission in the Compton-thick AGN set selected in the hard X-ray band (see also Sect. 5). This is in line with the noticeably large fraction of water masers (50%) found by Castangia et al. (2019), who studied a sample of heavily absorbed AGN, including CT sources, that were selected through a combination of mid-IR and X-ray data. We note that all CT AGN in the INTEGRAL sample show evidence of an association with discs (sometimes accompanied by jet and outflow components), except for Mkn 3, which is tentatively associated with a jet origin only (a core plus jet component is seen in the radio continuum maps of this source, Chiaraluce et al. 2020). When we exclude Mkn 3, the fraction of disc masers in CT is $50 \pm 17\%$. The interesting question here is why some sources are able to develop strong maser emission while others are not. In other words, if all Compton-thick AGN are potentially water maser emitters, why are only half of them able to reach luminosities high enough (above $10^{33} \text{ erg cm}^{-2} \text{ s}^{-1}$, see Fig. 3) for the current generation of radio receivers?

Masini, & Comastri (2018) have estimated that the expected disc water maser detection fraction among type 2 Seyferts in a volume-limited survey is about 10% to 20%. This value has been obtained by comparing the torus and maser disc covering factors (see their equation 2.1) and assuming that a maser disc is detected when the line of sight angle ranges between $90 \pm 10^\circ$ with respect to the polar axis and defining the probability of detecting a maser disc in a type 2 AGN as the ratio of the maser disc covering factor with respect to the torus one. This assumption might be inverted considering a covering factor for the CT part of the torus as derived from X-ray arguments (Ricci et al. 2017) to be $\sim 23\%$ (which also agrees with IR arguments, e.g. Hönig 2018) and using the information on the ratio between the water maser and CT covering factors to be 50%, to finally derive the expected maser disc inclination angle to range between 82 and 87° . These values agree with the observed disc angles in well-known disc

masers (Kuo et al. 2011; König et al. 2012), which confirms the idea that the masing disc is only a portion of the total CT medium (for a sketch of the possible geometry discussed here, see Fig. 2 in Masini et al. 2016). The maser covering factor could be considered as a lower limit when we assume the presence of warped discs, which is expected to increase the probability of intercepting maser emission (Darling 2017). Similarly, the known water maser variability might contribute to a possible non-detection if the masers flux decreases below the instrument sensitivity and therefore to an underestimate of the covering factor. Other effects contribute to our uncertainties in these estimates, for instance, X-ray scattering in clumpy media might dilute the true line-of-sight column density and thus prevent us from deriving unbiased orientation information (Ramolla et al. 2011). Despite the uncertainties involved, it is important to stress that the 50% detection fraction in Compton-thick AGN can in principle be explained in terms of a geometrical effect (i.e. proper opening angles of torus and maser disc and their relative alignment) and may not be due to peculiarities of individual objects.

9. Conclusions

Notwithstanding the valuable science that can be derived for AGN and cosmological studies, water megamasers are rarely found in galaxy surveys (e.g. Braatz et al. 2018). We here selected a sample of hard X-ray AGN detected above 20 keV by INTEGRAL/IBIS and searched for water megamaser emission among them in the literature and through our new dedicated observations (where one new maser detection was obtained). Of the 380 sources of the sample, only 51% have been observed at 22 GHz. In $15\pm 3\%$ of them, a detection was made. We also considered a sub-sample of 87 sources, limited in volume and statistically complete, and found that the detection fraction increases to $19\pm 5\%$. Most observed sources are at low redshift, and this is reflected by the observed detection fraction, which decreases with increasing redshift. This likely introduces a bias in our sample.

So far, the detection rates observed in large surveys of optically selected galaxies were about a few percent, which could only be improved by carefully selecting smaller samples on the basis of IR (8-22%; Hagiwara et al. 2002; 2003; Henkel et al. 2005) or a combination of mid-IR and X-ray data (50%; Castangia et al. 2019). Therefore, the hard X-ray selection provides one of the highest rates ever observed so far.

These fractions increase in type 2 Seyfert galaxies ($22\pm 5\%$), in particular in CT AGN, about 50% of which host water maser discs. This clearly indicates that the X-ray obscuring gas is related to the maser dusty medium. A comparison between the covering factor of the CT obscuring medium and the fraction of water masers in CT sources confirms the idea that the masing disc might only be a portion of the CT obscuring medium and that an edge-on line of sight ($i > 82$ degrees) is required for the water maser emission to be detected.

A possible decrease in detection fraction is observed as the hard X-ray luminosity increases, suggesting that a highly luminous nuclear environment might not favour maser emission. However, this result can be confirmed by completing the sample observations at higher luminosity. On the other hand, no significant correlation between the water maser and X-ray and hard X-ray luminosities has been found, while the marginally significant correlation between the water maser luminosity and the X-ray column density simply reflects the connection between the X-ray obscuring and the masing media.

All types of water masers are found by the soft gamma-ray selection of sources. Interestingly, all of the few water masers detected in type 1 AGN are jet or outflow candidates, while in type 2 AGN all types of masers are detected. This suggests that the dusty water maser medium is not solely associated with a classical obscuring torus, but might also reside in polar outflows or jets. This implies a more complex geometry, as envisaged by recent IR interferometric studies (see Hönic et al. 2018).

Overall, we conclude that hard X-ray samples of AGN provide the opportunity of significantly increasing the maser detection efficiency compared to previous surveys. Extremely high detection fractions (up to 50%) can be reached by targeting type 2 or heavily absorbed AGN that are nearby and in an optimised luminosity range. The discovery of new heavily absorbed sources with the increased sensitivity of the ongoing INTEGRAL/IBIS and Swift/BAT surveys together with the wealth of new sources that the eROSITA survey (Merloni 2018) will discover below 10 keV will offer the possibility to largely increase the samples for future water maser searches, and hopefully, detections.

Acknowledgements

The authors wish to thank the referee for her/his valuable comments that considerably improved our manuscript. AT and PC would like to thank Jim Braatz for providing information on some of the maser sources, prior to publication. FP, AM, LB, AB and PU acknowledge financial support from ASI under contract INTEGRAL ASI/INAF n.2019-35-HH. We acknowledge the help of 3 high school students (Alice Bizzarri, Andrea Cocozza and Fulvio Talarico) in the analysis of the BAT 70 m sample; they all participated in a summer stage at OAS/INAF Bologna during 2016. This project, being partly conducted by amateur astronomers under the supervision of professional scientists, represents a nice example on how citizen science work can help in dealing with a large data set.

References

- Alonso-Herrero, A., Pereira-Santaella, M., García-Burillo, S., et al. 2018, ApJ, 859, 144
- Antonucci, R. R. J., & Miller, J. S. 1985, ApJ, 297, 621
- Ballo, L., Severgnini, P., Braito, V., et al. 2015, A&A, 581, A87
- Baumgartner, W. H., Tueller, J., Markwardt, C. B., et al. 2013, ApJS, 207, 19
- Bennert, N., Schulz, H., & Henkel, C. 2004, A&A, 419, 127
- Bennert, N., Barvainis, R., Henkel, C., et al. 2009, ApJ, 695, 276
- Bird, A. J., Malizia, A., Bazzano, A., et al. 2007, ApJS, 170, 175
- Bird, A. J., Bazzano, A., Malizia, A., et al. 2016, ApJS, 223, 15
- Braatz, J. A., Wilson, A. S., & Henkel, C. 1996, ApJS, 106, 51
- Braatz, J. A., Wilson, A. S., & Henkel, C. 1997, ApJS, 110, 321
- Braatz, J. A., Reid, M. J., Greenhill, L. J., et al. 2008, *Frontiers of Astrophysics: A Celebration of Rao's 50th Anniversary*, 103
- Braatz, J. A., & Gugliucci, N. E. 2008, ApJ, 678, 96
- Braatz, J. 2008, *A Decade of Dark Energy*, 5
- Braatz, J. A., Reid, M. J., Humphreys, E. M. L., et al. 2010, ApJ, 718, 657
- Braatz, J., Condon, J., Constantin, A., et al. 2015, IAU General Assembly 29, 2255730
- Braatz, J., Pesce, D., Condon, J., et al. 2018, *Science with a Next Generation Very Large Array*, 821
- Castangia, P., Panessa, F., Henkel, C., et al. 2013, MNRAS, 436, 3388
- Castangia, P., Surcis, G., Tarchi, A., et al. 2019, A&A, 629, A25
- Chiaraluca, E., Panessa, F., Bruni, G., et al. 2020, MNRAS, 495, 3943
- Darling, J. 2017, ApJ, 837, 100
- Davies, R. I., Maciejewski, W., Hicks, E. K. S., et al. 2014, ApJ, 792, 101
- Decarli, R., Dottì, M., Fontana, M., et al. 2008, MNRAS, 386, L15
- Diamond-Stanic, A. M., Rieke, G. H., & Rigby, J. R. 2009, ApJ, 698, 623
- Elitzur, M. 1992, *Astrophysics and Space Science Library*
- Elitzur, M., & Shlosman, I. 2006, ApJ, 648, L101
- Fukumura, K., Kazanas, D., Shrader, C., et al. 2018, ApJ, 853, 40
- Gallimore, J. F., Baum, S. A., O'Dea, C. P., et al. 1996, ApJ, 458, 136

- Gallimore, J. F., Henkel, C., Baum, S. A., et al. 2001, *ApJ*, 556, 694
- Gear, W. K., Stevens, J. A., Hughes, D. H., et al. 1994, *MNRAS*, 267, 167
- Gehrels, N., Chincarini, G., Giommi, P., et al. 2004, *ApJ*, 611, 1005
- Gofford, J., Reeves, J. N., McLaughlin, D. E., et al. 2015, *MNRAS*, 451, 4169
- Gray, M. D., Baudry, A., Richards, A. M. S., et al. 2016, *MNRAS*, 456, 374
- Greenhill, L. J., Ellingsen, S. P., Norris, R. P., et al. 2002, *ApJ*, 565, 836
- Greenhill, L. J., Kondratko, P. T., Lovell, J. E. J., et al. 2003a, *ApJ*, 582, L11
- Greenhill, L. J., Booth, R. S., Ellingsen, S. P., et al. 2003b, *ApJ*, 590, 162
- Greenhill, L. J., Tilak, A., & Madejski, G. 2008, *ApJ*, 686, L13
- Greenhill, L. J., Kondratko, P. T., Moran, J. M., et al. 2009, *ApJ*, 707, 787
- Guilloteau, S., & Lucas, R. 2000, *Imaging at Radio Through Submillimeter Wavelengths*, 299
- Hagiwara, Y., Diamond, P. J., & Miyoshi, M. 2002, *A&A*, 383, 65
- Hagiwara, Y., Diamond, P. J., Miyoshi, M., et al. 2003, *MNRAS*, 344, L53
- Hagiwara, Y., & Edwards, P. G. 2015, *ApJ*, 815, 124
- Henkel, C., Guesten, R., Downes, D., et al. 1984, *A&A*, 141, L1
- Henkel, C., Peck, A. B., Tarchi, A., et al. 2005, *A&A*, 436, 75
- Herrnstein, J. R., Moran, J. M., Greenhill, L. J., et al. 1997, *ApJ*, 475, L17
- Humphreys, E. M. L., Vlemmings, W. H. T., Impellizzeri, C. M. V., et al. 2016, *A&A*, 592, L13
- Hönig, S. F., Alonso Herrero, A., Gandhi, P., et al. 2018, *Experimental Astronomy*, 46, 413
- Jarosik, N., Bennett, C. L., Dunkley, J., et al. 2011, *ApJS*, 192, 14
- Kamali, F., Henkel, C., Brunthaler, A., et al. 2017, *A&A*, 605, A84
- Kameno, S., Nakai, N., Sawada-Satoh, S., et al. 2005, *ApJ*, 620, 145
- Kondratko, P. T., Greenhill, L. J., & Moran, J. M. 2005, *ApJ*, 618, 618
- Kondratko, P. T., Greenhill, L. J., Moran, J. M., et al. 2006a, *ApJ*, 638, 100
- Kondratko, P. T., Greenhill, L. J., & Moran, J. M. 2006b, *ApJ*, 652, 136
- Kuo, C. Y., Braatz, J. A., Condon, J. J., et al. 2011, *ApJ*, 727, 20
- Kuo, C. Y., Constantin, A., Braatz, J. A., et al. 2018, *ApJ*, 860, 169
- Kylafis, N. D., & Norman, C. A. 1991, *ApJ*, 373, 525
- König, S., Eckart, A., Henkel, C., et al. 2012, *MNRAS*, 420, 2263
- Leipski, C., Falcke, H., Bennert, N., et al. 2006, *A&A*, 455, 161
- Liu, Z. W., Zhang, J. S., Henkel, C., et al. 2017, *MNRAS*, 466, 1608
- Lo, K. Y. 2005, *ARA&A*, 43, 625
- Malizia, A., Stephen, J. B., Bassani, L., et al. 2009, *MNRAS*, 399, 944
- Malizia, A., Bassani, L., Bazzano, A., et al. 2012, *MNRAS*, 426, 1750
- Malizia, A., Landi, R., Molina, M., et al. 2016, *MNRAS*, 460, 19
- Maloney, P. R. 2002, *PASA*, 19, 401
- Masini, A., Comastri, A., Baloković, M., et al. 2016, *A&A*, 589, A59
- Masini, A., & Comastri, A. 2018, *Astrophysical Masers: Unlocking the Mysteries of the Universe*, 133
- Mathur, S. 2000, *MNRAS*, 314, L17
- Mehdipour, M., Kaastra, J. S., Kriss, G. A., et al. 2017, *A&A*, 607, A28
- Merloni, A. 2018, *AGN13: Beauty and the Beast*, 71
- Miyoshi, M., Moran, J., Herrnstein, J., et al. 1995, *Nature*, 373, 127
- Morganti, R., Tsvetanov, Z. I., Gallimore, J., et al. 1999, *A&AS*, 137, 457
- Neufeld, D. A., Maloney, P. R., & Conger, S. 1994, *ApJ*, 436, L127
- Oh K., et al., 2018, *ApJS*, 235, 4
- Orienti, M., & Prieto, M. A. 2010, *MNRAS*, 401, 2599
- Ott, J., Meier, D. S., McCoy, M., et al. 2013, *ApJ*, 771, L41
- Padovani, P., Alexander, D. M., Assef, R. J., et al. 2017, *A&A Rev.*, 25, 2
- Panessa, F., de Rosa, A., Bassani, L., et al. 2011, *MNRAS*, 417, 2426
- Panessa, F., & Giroletti, M. 2013, *MNRAS*, 432, 1138
- Peck, A. B., Henkel, C., Ulvestad, J. S., et al. 2003, *ApJ*, 590, 149
- Pesce, D. W., Braatz, J. A., Condon, J. J., et al. 2015, *ApJ*, 810, 65
- Ramolla, M., Haas, M., Bennert, V. N., et al. 2011, *A&A*, 530, A147
- Reid, M. J., Braatz, J. A., Condon, J. J., et al. 2009, *ApJ*, 695, 287
- Ricci, C., Trakhtenbrot, B., Koss, M. J., et al. 2017, *Nature*, 549, 488
- Sato, N., Yamauchi, A., Ishihara, Y., et al. 2005, *PASJ*, 57, 587
- Schnorr-Müller, A., Storchi-Bergmann, T., Robinson, A., et al. 2016, *MNRAS*, 457, 972
- Tarchi, A., Henkel, C., Chiaberge, M., et al. 2003, *A&A*, 407, L33
- Tarchi, A., Castangia, P., Henkel, C., et al. 2011a, *A&A*, 525, A91
- Tarchi, A., Castangia, P., Columbano, A., et al. 2011b, *A&A*, 532, A125
- Tarchi, A. 2012, *Cosmic Masers - from OH to H₂O*, 323
- Tilak, A., Greenhill, L. J., Done, C., et al. 2008, *ApJ*, 678, 701
- Tueller, J., Mushotzky, R. F., Barthelmy, S., et al. 2008, *ApJ*, 681, 113
- Ubertini, P., Lebrun, F., Di Cocco, G., et al. 2003, *A&A*, 411, L131
- van den Bosch, R. C. E., Greene, J. E., Braatz, J. A., et al. 2016, *ApJ*, 819, 11
- Vulic, N., Hornschemeier, A. E., Wik, D. R., et al. 2018, *ApJ*, 864, 150
- Wang, J., Zhang, J.-S., & Fan, J.-H. 2010, *Research in Astronomy and Astrophysics*, 10, 915
- Yamashita, T., Komugi, S., Matsuhara, H., et al. 2017, *ApJ*, 844, 96
- Zhang, J. S., Henkel, C., Guo, Q., et al. 2012, *A&A*, 538, A152
- Zhang, J. S., Liu, Z. W., Henkel, C., et al. 2017, *ApJ*, 836, L20
- Zhang, J. S., Henkel, C., Kadler, M., et al. 2006, *A&A*, 450, 933
- Zhu, G., Zaw, I., Blanton, M. R., et al. 2011, *ApJ*, 742, 73

Appendix A: Tables with the total sample and detection fractions in the Swift/BAT and Diamond-Stanic samples

Table 1A lists all 380 INTEGRAL/IBIS AGN with their optical coordinates, redshift, class, hard X-ray (20–100 keV) flux, X-ray (2–10 keV) flux, X-ray column density, a note to indicate whether the source was observed at 22 GHz, which maser type was detected, and respective references. Finally, for sources for which maser emission was detected, we also list the reported water maser isotropic luminosity and the reference to the maser data; for objects observed at 22 GHz but without a detected maser, we report the 1σ rms and an upper limit to the maser luminosity. Objects belonging to the complete sample are highlighted in boldface in Table 1A for clarity.

In Table 2A we report the 17 detected sources from the Swift/BAT 9 catalogue with their names, optical classification as type 1 or 2 AGN, and coordinates. Analogously, in Table 3A, the 21 AGN detected at 22 GHz from the Diamond-Stanic et al. (2009) sample are reported.

Table 2A: AGN in the BAT 9-month survey sample with water maser detections

Name (class)	RA(J2000), Dec(J2000)	Name (class)	RA(J2000), Dec(J2000)
NGC235A(2)	00 42 52.81, -23 32 27.7	NGC4945(2)	13 05 27.28, -49 28 04.4
Mkn348(2)	00 48 47.10, +31 57 25.0	NGC5128(2)	13 25 27.61, -43 01 08.8
MKN3(2)	06 15 36.31, +71 02 14.9	NGC5506(2)	14 13 14.87, -03 12 27.0
NGC3081(2)	09 59 29.54, -22 49 34.6	NGC5728(2)	14 42 23.90, -17 15 11.0
NGC3783(1)	11 39 01.78, -37 44 01.7	NGC6240(2)	16 52 58.97, +02 24 01.7
NGC4051(1)	12 03 09.62, +44 31 52.8	NGC6300(2)	17 16 59.47, -62 49 14.0
NGC4151(1)	12 10 32.66, +39 24 20.7	ESO103-G35(2)	18 38 20.30, -65 25 41.0
Mrk766(1)	12 18 26.48, +29 18 14.0	3C403(2)	19 52 15.82, +02 30 24.3
NGC4388(2)	12 25 46.93, +12 39 43.3		

Table 3A: Maser galaxies in the Diamond-Stanic et al. (2009) sample

Name (class)	RA(J2000), Dec(J2000)	Name(class)	RA(J2000), Dec(J2000)
NGC1068(2)	02 42 40.70, -00 00 48.0	NGC4258(2)	12 18 57.62, +47 18 14.0
NGC1386(2)	03 36 46.24, -35 59 57.0	NGC4388(2)	12 25 46.93, +12 39 43.3
NGC2273(2)	06 50 08.67, +60 50 44.8	NGC4945(2)	13 05 27.28, -49 28 04.4
NGC2639(2)	08 43 38.09, +50 12 19.9	NGC5128(2)	13 25 27.61, -43 01 08.8
NGC3081(2)	09 59 29.54, -22 49 34.6	Circinus(2)	14 13 08.90, -65 20 27.0
NGC3079(2)	10 01 57.80, +55 40 47.2	NGC5506(2)	14 13 14.87, -03 12 27.0
IC2560(2)	10 16 18.71, -33 33 49.7	NGC5643(2)	14 32 40.70, -44 10 28.0
NGC3735(2)	11 35 57.33, +70 32 08.1	NGC5728(2)	14 42 23.90, -17 15 11.0
NGC3783(1)	11 39 01.78, -37 44 01.7	NGC6300(2)	17 16 59.47, -62 49 14.0
NGC4051(1)	12 03 09.62, +44 31 52.8	NGC7479(2)	23 04 56.67, +12 19 22.4
NGC4151(1)	12 10 32.66, +39 24 20.7		

Table A.1: Table 1A: Galaxies detected by *INTEGRAL*/*IBIS*.

Name	RA	Dec	z	Class	$F_{\text{H}\alpha}^*$	F_X	$\text{Log } N_{\text{H}}$	Notes	Rms*	$L_{\text{H}\alpha}^{**}$	Ref.***
IGR J00040+7020	00 04 01.92	+70 19 18.5	0.096	Sy2	1.47	0.35	22.52				
IGR J00158+5605	00 15 54.19	+56 02 57.5	0.169	Sy1.5	<0.66	0.31	21.50				
IGR J00256+6821	00 25 32.50	+68 21 44.0	0.012	Sy2	1.47	0.05	23.60				
IGR J00333+6122	00 33 18.34	+61 27 43.3	0.105	Sy1.5	1.38	0.68	21.93	0	2	<14.0	this work
SWIFT J0034.5-7904	00 34 16.7	-79 05 20	0.07400	Sy1	1.09	6.33	23.49	0	2	<9.4	this work
IES 0033+595	00 35 52.60	+59 50 05.0	0.086	BL Lac	1.83	5.90	21.55				
IGR J00465-4005	00 46 20.68	-40 05 49.1	0.201	Sy2	3.56	0.12	23.38				
MKN 348	00 48 47.10	+31 57 25.0	0.015	Sy2	10.60	0.44	23.02	M(J,a)	4	142±28	P03
Mrk 352	00 59 53.3	+31 49 37	0.01486	Sy1	3.21	11.89	20.72	0	4	<0.6	MCP
Mrk 1152	01 13 50.1	-14 50 44	0.05271	Sy1.5	2.94	4.66	20.25	0	4	<7.0	MCP
Fairall 9	01 23 45.8	-58 48 21	0.04702	Sy1.2	3.34	7.40	20.50	0	3	<0.7	MCP
NGC 526A	01 23 54.40	-35 03 56.0	0.019	Sy1.9	5.34	1.80	22.23	0	3	<0.7	MCP
RX J0137.7+5814	01 37 50.49	+58 14 11.0	-	BL Lac	<0.68	1.01	21.60				
ESO 297-18	01 38 37.10	-40 00 41.0	0.025	Sy2	6.08	0.33	23.70	0	16(1.3)	<27.4	K06
IGR J01528-0845	01 52 48.4	-08 43 21	0.03697	Sy2 ^s	0.85	0.40	23.49	0	4	<3.5	MCP
IGR J01528-0326	01 52 49.00	-03 26 48.5	0.017	Sy2	2.60	0.40	23.15	0	3	<0.5	MCP
IGR J01545+6437	01 54 35.29	+64 37 57.5	0.034	Sy2	<0.83	0.0097	21.82	0	6	<4.4	MCP
Mrk 584	02 00 26.3	+02 40 10	0.07877	Sy1.8	1.79	3.98	20.47				
NGC 788	02 01 06.40	-06 48 56.0	0.0136	Sy2	6.00	0.61	23.48	0	3	<0.4	MCP
Mrk 1018	02 06 16.00	-00 17 29.0	0.0424	Sy1	1.70	1.19	20.41	0	3	<3.4	MCP
IGR J02086-1742	02 08 34.95	-17 39 34.8	0.129	Sy1.2	2.75	0.64	<20.23				
IGR J02097+5222	02 09 34.30	+52 22 48.0	0.0492	Sy1	2.81	1.30	21.23	0	6	<9.2	MCP
Mrk 590	02 14 33.50	-00 46 00.0	0.02638	Sy1	1.46	0.64	20.42	0	3	<1.3	MCP
SWIFT J0216.3+5128	02 16 26.73	+51 25 25.1	0.422	Sy2?	1.62	1.27	22.104				
SWIFT J0218.0+7348	02 17 30.83	+73 49 32.5	2.367	QSO/bl	2.70	0.55	21.54				
Mrk 1040	02 28 14.50	+31 18 42.0	0.0166	Sy1.5	5.19	0.51	20.56	0	3	<0.5	MCP
IGR J02341+0228	02 33 49.0	+02 29 25	0.32100	QSO	1.55	2.90	20.40				
IGR J02343+3229	02 34 20.10	+32 30 20.0	0.0162	Sy2/L	4.74	0.82	22.34	0	4	<0.7	MCP
NGC 985	02 34 37.80	-08 47 15.0	0.043	Sy1.5	2.38	5.40	20.50	0	3	<3.5	MCP
NGC 1052	02 41 04.80	-08 15 21.0	0.005	Sy2/L	1.69	0.40	23.30	M(J,a)		208±16	K05
RBS 345	02 42 14.60	+05 30 36.0	0.069	Sy1	2.02	0.26	20.72				
NGC 1068	02 42 40.70	-00 00 48.0	0.0038	Sy2	2.36	0.50	25.00	M(D+J,a)	4	155±5	G96
QSO B0241+62	02 44 57.69	+62 28 06.5	0.044	Sy1.2	5.17	3.6	21.32	0	4	<4.9	MCP
MCG -07-06-018	02 46 37.00	-42 22 01.0	0.0696	XBONG	3.72	0.007	>24				
SWIFT J0249.1+2627	02 48 59.3	+26 30 39	0.05800	Sy2	1.90	3.73	23.43	0	3	<6.4	MCP
IGR J02504+5443	02 50 42.59	+54 42 17.7	0.015	Sy2	1.87	0.48	21.62	0	3	<0.4	MCP
MCG -02-08-014	02 52 23.40	-08 30 37.0	0.0167	Sy2?	1.88	1.20	23.08	0	5	<0.9	MCP
NGC 1142	02 55 12.20	-00 11 01.0	0.0288	Sy2	6.12	0.42	23.80	0	2	<1.0	MCP
MCG-02-08-038	03 00 04.3	-10 49 29	0.03259	Sy1	1.81	16.7	21.56				
NGC 1194	03 03 49.10	-01 06 13.0	0.0136	Sy2	2.57	0.09	24.20	M(D,a)		131±7	P15
PKS 0312-770	03 11 55.2	-76 51 51	0.22519	Sy1/QSO	1.21	2.19	20.93				
B3 B0309+411B	03 13 01.96	+41 20 01.2	0.136	Sy1	<2.49	2.36	21.11	0	3	<35.1	this work
SWIFT J0318.7+6828	03 18 19.02	+68 29 32.1	0.0901	Sy1.9	<0.91	0.73	22.61				
NGC 1275	03 19 48.16	+41 30 42.1	0.0175	Sy1.5/L	3.82	1.23	21.08	0	9	<1.7	MCP

Table A.1.: continue

Name	RA	Dec	z	Class	F_{HX}^i	F_X^i	$\log N_H$	Notes	Rms*	L_{H2O}^{**}	Ref.**
IH 0323+342	03 24 41.16	+34 10 45.8	0.061	NLSy1	3.96	0.64	21.16				
IGR J03249+4041-SW	03 25 13.20	+40 41 55.0	0.0477	Sy2	1.35	0.12	>21.18				
IGR J03249+4041-NE	03 25 12.20	+40 42 02.0	0.0475	Sy2	1.35	0.09	22.48				
IGR J03334+3718	03 33 18.79	+37 18 11.1	0.05583	Sy1.5	2.61	0.61	21.15				
NGC 1365	03 33 36.31	-36 08 27.8	0.0054	Sy1.9	4.10	1.30	24.65	O	3	<0.1	MCP
NRAO 140	03 36 30.10	+32 18 29.0	1.2580	QSO/bl	2.46	0.72	21.10				
ESO 548-G81	03 42 03.7	-21 14 40.0	0.0145	Sy1	4.45	1.35	20.36	O	5	<0.7	MCP
IGR J03532-6829	03 52 57.00	-68 31 18.0	0.087	BL Lac	<8.52	1.75	20.95				
SWIFT J0353.7+3711	03 53 42.5	+37 14 07	0.01865	Sy2/L	0.89	3.50	22.57	O	5	<1.1	MCP
4C +62.08	03 55 40.2	+62 40 59	1.10900	Sy1	1.30	0.45	21.51				
SWIFT J0357.6+4153	03 57 45.1	+41 55 05	0.05300	Sy1.9	1.55	5.88	22.30				
3C 098	03 58 55.00	+10 26 24.0	0.0304	Sy2	3.96	0.27	23.08	O	2	<1.2	MCP
4C03.8	04 07 16.45	+03 42 25.9	0.089	Sy2	3.45	0.21	23.45				
3C 111	04 18 21.28	+38 01 35.8	0.0485	Sy1	10.40	3.51	21.66	O	8	<11.9	this work
IGR J04221+4856	04 22 00.50	+48 56 04.0	0.114	Sy1	1.42	-	21.85				
LEDA 15023	04 23 40.80	+04 08 03.0	0.045	Sy2	1.87	0.13	23.48	O	6	<7.7	MCP
3C120	04 33 11.09	+05 21 15.6	0.033	Sy1.5	7.98	4.60	21.20	O	6	<4.1	MCP
UGC 3142	04 43 46.89	+28 58 19.0	0.0216	Sy1	4.87	1.70	22.60	O	5	<1.5	MCP
SWIFT J0444.1+2813	04 44 09.0	+28 13 01	0.01127	Sy2	1.49	12.34	22.53	O	3	<0.2	MCP
SWIFT J0450.7-5813	04 51 44.0	-58 11 01	0.09070	Sy1.5	1.85	4.74	20.95				
MCG -01-13-025	04 51 41.5	-03 48 33	0.01589	Sy1.2	1.47	21.3	20.54	O	6	<1.0	MCP
LEDA 168563	04 52 04.79	+49 32 44.6	0.029	Sy1	5.55	4.52	21.73	O	4	<2.1	MCP
SWIFT J0453.4+0404	04 53 25.74	+04 03 41.6	0.0296	Sy2	2.19	0.20	24.16	O	3	<1.7	MCP
ESO 033-G02	04 55 59.05	-75 32 28.3	0.0181	Sy2	2.42	1.59	22.10	O	15 (1.3)	<13.5	K06
LEDA 075258	05 02 09.00	+03 31 50.0	0.01599	Sy1	1.26	0.55	19.75	O	59	<9.5	B96
SWIFT J0505.8-2348	05 05 45.70	-23 51 14.0	0.03504	Sy2	5.49	1.36	23.50	O	4	<3.1	MCP
IGR J05081+1722	05 08 19.7	+17 21 48	0.01750	Sy2	1.25	6.45	22.38	M(?)		35±10	MCP
4U 0517+17	05 10 45.50	+16 29 55.0	0.0179	Sy1.5	6.83	2.53	20.95	O	5	<1.0	MCP
SWIFT J0515.3+1854	05 15 19.8	+18 54 52	0.02349	Sy2	1.81	1.91	23.06	O	4	<1.4	MCP
Ark 120	05 16 11.48	-00 09 00.6	0.0327	Sy1	6.55	2.87	20.99	O	45 (0.66)	<67.0	B96
SWIFT J0516.3+1928	05 16 22.7	+19 27 11	0.02115	Sy2	1.53	1.80	22.64				
SWIFT J0519.5-3140	05 19 35.81	-32 39 28.0	0.0126	Sy1.5	4.34	0.34	23.42	O	4	<0.4	MCP
PICTOR A	05 19 49.69	-45 46 44.5	0.0351	Sy1/L	<3.36	1.13	20.78	O	14 (1.3)	<47.3	K06
PKS 0521-36	05 22 58.00	-36 27 31.0	0.0565	Sy1	2.19	1.10	20.55	O	5	<10.1	MCP
PKS 0528+134	05 30 56.42	+13 31 54.9	2.060	QSO/bl	1.50	2.57	21.38				
QSO J0539-2839	05 39 54.3	-28 39 56.0	3.1040	QSO/bl	1.74	0.17	21.20				
SWIFT J0544.4+5909	05 44 22.6	+59 07 36	0.06597	Sy1.9	2.00	5.25	22.26				
IGR J05470+5034	05 47 14.9	+50 38 25	0.03600	Sy2	1.19	1.40	23.18	O	3	<0.1	MCP
NGC 2110	05 52 11.38	-07 27 22.4	0.0078	Sy2	17.90	2.50	22.46	O	4	<1.1	MCP
MCG+08-11-011	05 54 53.63	+46 26 21.8	0.0205	Sy1.5	8.46	5.62	21.32	O	5	<3.6	MCP
4U 0557-385	05 58 02.05	-38 20 04.6	0.0339	Sy1.2	<2.76	2.00	22.11	O	4	<2.8	MCP
IRAS 05589+2828	06 02 09.70	+28 28 17.0	0.033	Sy1	4.02	1.64	21.66				
SWIFT J0601.9-8636	06 05 39.60	-86 37 54.0	0.0064	Sy2	2.59	0.11	24.00				
IGR J06058-2755	06 05 48.96	-27 54 40.1	0.0900	Sy1.5	1.98	0.66	20.38				

Table A.1.: continue

Name	RA	Dec	z	Class	F_{HX}^{\dagger}	F_X^{\dagger}	Log N_H	Notes	Rms*	L_{H2O}^{**}	Ref.***
Mrk 3	06 15 36.31	+71 02 14.9	0.0135	Sy2	9.53	0.65	24.00	M(J?,b)		5±5	MCP
IGR J06233-6436	06 23 07.70	-64 36 20.0	0.12889	Sy1	1.56	0.46	20.59				
IGR J06239-6052	06 23 45.61	-60 58 45.4	0.0405	Sy2	<0.98	0.32	23.28				
SWIFT J0623.8-3215	06 23 46.4	-32 13 00	0.02243	Sy2	1.94	1.16	23.91	O	4	<1.3	MCP
PKS 0637-752	06 35 46.5	-75 16 17	0.65300	QSO/bl	1.66	4.72	21.10				
SWIFT J0640.4-2554	06 40 11.69	-25 53 43.4	0.0248	Sy1.2	3.83	1.88	21.38	O	13 (1.3)	<21.9	K06
IGR J06415+3251	06 41 23.00	+32 55 39.0	0.01719	Sy2	4.74	0.33	23.20	O	3	<0.6	MCP
Mrk 6	06 52 12.36	+74 25 37.2	0.0188	Sy1.5	4.32	2.51	22.90	O	3	<0.7	MCP
IGR J06523+5334	06 52 31.41	+53 34 31.5	0.301	Sy1.2/QSO	<4.83	0.02	20.81				
SWIFT J0709.3-1527	07 09 12.3	-15 27 00	0.13900	BL Lac	<1.25	13.6	21.76				
IGR J07225-3810	07 22 22.4	-38 14 55	1.023	QSO/bl	2.08	0.58	21.33				
PKS 0723-008	07 25 50.6	-00 54 57	0.12800	BL Lac	1.58	4.97	21.10				
LEDA 96373	07 26 26.30	-35 54 21.0	0.0294	Sy2	2.25	0.05	22.84				
Mrk 79	07 42 32.8	+49 48 35	0.02219	Sy1.2	4.89	15.8	20.72	O	4	<1.2	MCP
IGR J07565-4139	07 56 19.62	-41 37 42.1	0.021	Sy2	1.43	0.32	21.86	O	10	<2.8	this work
IGR J07597-3842	07 59 41.82	-38 43 56.0	0.04	Sy1.2	3.51	2.37	21.78	O	5	<5.1	this work
ESO 209-12	08 01 57.60	-49 46 42.0	0.0405	Sy1.5	2.25	8.30	21.38				
Mrk 1210	08 04 05.8	+05 06 50	0.01350	Sy2	5.96	9.70	23.52	M(D,c)		160±30	MCP
PG0804+761	08 10 58.65	+76 02 42.5	0.1	Sy1	<1.53	1.00	20.70				
IGR J08190-3835	08 19 11.36	-38 33 10.5	0.009	Sy2	1.36	0.15	23.13				
FRL 1146	08 38 30.70	-35 59 35.0	0.0316	Sy1.5	2.10	1.26	21.45	O	7	<4.4	this work
QSO B0836+710	08 41 24.36	+70 53 42.1	2.172	QSO/bl	5.77	2.63	20.47				
SWIFT J0845.0-3531	08 45 21.4	-35 30 24	0.13700	Sy1.2	1.11	4.64	22.38				
IGR J08557+6420	08 55 12.54	+64 23 45.5	0.037	Sy2?	1.74	0.28	23.29	O	14	<12.1	MCP
IGR J08558+0814	08 55 58.60	+08 13 19.0	0.22	Sy1	<3.49	0.0065	20.67				
Mrk 18	09 01 58.4	+60 09 06	0.01109	Sy2	2.62	1.57	23.26	O	4	<0.3	MCP
IGR J09025-6814	09 02 39.46	-68 13 36.6	0.014	XBONG	1.96	0.92	22.90				
IGR J09026-4812	09 02 37.31	-48 13 33.9	0.0391	Sy1	2.42	0.46	22.34				
IRXS J09043.1-382920	09 04 33.3	-38 29 22	0.01603	Sy1	0.92	0.92	21.46				
SWIFT J0917.2-6221	09 16 09.41	-62 19 29.5	0.0573	Sy1	1.91	1.43	21.61				
IGR J09189-4418	09 18 58.8	-44 18 30	-	AGN	0.53	2.30	22.66				
MCG-01-24-012	09 20 46.31	-08 03 21.9	0.0196	Sy2	4.06	1.00	22.80	O	3	<0.7	MCP
Mrk 110	09 25 12.85	+52 17 10.5	0.0353	NLSy1	5.06	2.79	20.30	O	3	<2.3	MCP
IGR J09253+6929	09 25 47.56	+69 27 53.6	0.039	Sy1.5	<1.94	0.05	23.15				
SWIFT J0929.7+6232	09 29 37.8	+62 32 39	0.02561	Sy2	2.06	0.97	23.31	O	5	<2.1	MCP
IGR J09446-2636	09 44 37.02	-26 33 55.4	0.1425	Sy1.5	<2.34	0.5	20.81				
NGC 2992	09 45 42.05	-14 19 35.0	0.0077	Sy2	6.51	1.20	21.90	O	2	<0.1	MCP
MCG-05-23-016	09 47 40.17	-30 56 55.9	0.0085	Sy2	14.50	8.76	22.21	O	5	<0.2	MCP
4C 73.08	09 49 45.8	+73 14 23	0.05810	Sy2	1.17	1.81	23.96				
IGR J09523-6231	09 52 20.70	-62 32 37.0	0.252	Sy1.9	1.43	0.37	22.80				
M 81	09 55 33.2	+69 03 55	0.00084	Sy1.8/L	1.11	11.1	20.74	O	9	<0.004	MCP
NGC 3081	09 59 29.54	-22 49 34.6	0.0079	Sy2	5.91	0.13	23.82	M(?)		17±8	MCP
SWIFT J0959.7-3112	09 59 42.6	-31 12 58	0.03700	Sy1	2.21	7.18	20.80				
NGC 3079	10 01 57.8	+55 40 47	0.00372	Sy2	3.72	38.0	25.00	M(D+O,d)		230±40	MCP

Table A.1.: continue

Name	RA	Dec	z	Class	F_{HX}^+	F_X^+	Log N_H	Notes	Rms*	$L_{H_2O}^{**}$	Ref.***
SWIFT J1009.3-4250	10 09 48.22	-42 48 40.4	0.033	Sy2	2.81	0.31	23.41	O	10	<6.9	this work
IGR J10147-6354	10 14 15.55	-63 51 50.1	0.202	Sy1.2	<1.07	0.21	22.30				
NGC 3227	10 23 30.61	+19 51 53.8	0.0038	Sy1.5	11.30	0.81	22.83	O	3	<0.03	MCP
NGC 3281	10 31 52.06	-34 51 13.3	0.0107	Sy2	5.11	0.29	24.18	O	3	<0.2	MCP
SWIFT J1038.8-4942	10 38 45.20	-49 46 53.2	0.06	Sy1.5	2.00	1.45	21.79				
IGR J10404-4625	10 40 22.55	-46 25 25.7	0.024	Sy2	3.36	1.20	22.61				
MCG+04-26-006	10 46 42.67	+25 55 52.5	0.02	L	3.19	0.22	23.09	O	4	<1.0	MCP
Mrk 421	11 04 27.31	+38 12 31.8	0.0300	BL Lac	37.65	47.9	20.89	O	2	<1.1	MCP
NGC 3516	11 06 47.50	+72 34 07.0	0.0088	Sy1.5	5.55	2.3	22.50	O	4	<0.2	MCP
IGR J11366-6002	11 36 42.04	-60 03 06.6	0.014	Sy2/L	1.02	0.46	22.40				
NGC 3783	11 39 01.78	-37 44 18.7	0.0097	Sy1.5	13.30	6.03	22.06	M(?)		20±5	MCP
SWIFT J1143.7+7942	11 45 16.0	+79 40 53	0.00652	Sy1.2	2.21	6.51	20.00	O	4	<0.1	MCP
H1143-182	11 45 40.47	-18 27 15.5	0.0329	Sy1.5	<4.89	1.43	20.48	O	5	<3.4	MCP
PKS 1143-696	11 45 53.62	-69 54 01.8	0.244	Sy1.2	1.36	0.54	21.21				
B2 1144+35B	11 47 22.1	+35 01 08	0.06313	Sy1.9	1.21	3.09	20.23				
SWIFT J1200.8+0650	12 00 57.92	+06 48 23.1	0.0360	Sy2	1.72	0.58	22.92	O	3	<2.5	MCP
IGR J12026-5349	12 02 47.63	-53 50 07.7	0.028	Sy2	3.72	0.85	22.41				
NGC 4051	12 03 09.62	+44 31 52.8	0.0023	NLSy1	3.59	0.63	21.48	M(J/O,e)		2.6±0.2	T11
NGC 4074	12 04 29.65	+20 18 58.2	0.0224	Sy2	2.19	0.18	23.48	O	4	<1.3	MCP
Mrk 198	12 09 14.1	+47 03 30	0.02422	Sy2	1.09	5.12	23.00	O	4	<1.5	MCP
NGC 4138	12 09 29.79	+43 41 07.1	0.0030	Sy1.9	2.62	0.554	22.95	O	2	<0.01	MCP
NGC 4151	12 10 32.66	+39 24 20.7	0.0033	Sy1.5	30.50	25.00	23.34	M(J?,b)		1.0±0.5	MCP
IGR J12107+3822	12 10 44.27	+38 20 10.1	0.0229	Sy1.5	1.47	0.34	22.67	O	3	<1.0	MCP
IGR J12131+0700	12 12 49.81	+06 59 45.1	0.2095	Sy1.5-1.8	1.74	0.013	20.14				
NGC4235	12 17 09.91	+07 11 28.3	0.0080	Sy1.2	<0.94	0.28	21.20	O	6	<0.2	MCP
Mrk 766	12 18 26.48	+29 48 46.2	0.0129	NLSy1	1.81	1.33	21.95	M(J/O?,e)		9.1±0.7	T11
NGC 4258	12 18 57.5	+47 18 14.0	0.00149	Sy2	1.69	1.35	23.03	M(D,a)		89.7±0.2	P15
PKS 1217+02	12 20 11.9	+02 03 42	0.24023	Sy1.2	1.02	4.3	20.25				
PG 1218+305	12 21 21.9	+30 10 37	0.18365	BL Lac	0.92	0.26	20.29				
4C 0442	12 22 22.55	+04 13 15.8	0.965	QSO/bl	2.30	0.25	20.23				
Mrk 50	12 23 24.14	+02 40 44.8	0.0234	Sy1	<1.30	0.98	<21.08	O	4	<1.4	this work
PG 1222+216	12 24 54.4	+21 22 46	0.43200	QSO/bl	1.64	8.30	20.32				
NGC 4388	12 25 46.93	+12 39 43.3	0.0084	Sy2	24.60	2.30	23.44	M(D,a)		13±3	P15
NGC 4395	12 25 48.93	+33 32 47.8	0.00106	Sy2	2.090	0.62	22.72	O	4	<0.003	MCP
IGR J12288+0052	12 28 45.70	+00 50 19.0	0.5756	Sy2	<0.92	0.03	22.40				
3C 273	12 29 06.70	+02 03 08.6	0.1583	Sy1/QSO	19.46	9.62	20.23				
IGR J12319-0749	12 31 57.7	-07 47 18	3.66800	QSO/bl	0.98	5.70	20.23				
Mrk 771	12 32 03.6	+20 09 29	0.06301	Sy1	0.83	3.01	20.44				
XSS J12303-4232	12 32 11.8	-42 17 52	0.10000	Sy1.5	1.36	5.40	20.88				
NGC 4507	12 35 36.55	-39 54 33.3	0.0118	Sy2	16.30	1.28	23.88	O	10	<0.9	MCP
ESO 506-G27	12 38 54.40	-27 18 28.0	0.0250	Sy2	8.32	0.51	23.03	O	4	<1.6	MCP
SWIFT J1238.6+0928	12 38 43.4	+09 27 37	0.08290	Sy2	0.58	0.92	23.52				
LEDA 170194	12 39 06.32	-16 10 47.8	0.0367	Sy2	3.77	2.00	22.46	O	3	<2.6	MCP
NGC 4593	12 39 39.43	-05 20 39.3	0.009	Sy1	7.12	3.72	20.30	O	5	<0.3	MCP

Table A.1: continue

Name	RA	Dec	z	Class	F_{HX}^+	F_X^+	Log N_H	Notes	Rms*	$L_{H\alpha}^*$	Ref.**
IGR J12415-5750	12 41 25.74	-57 50 03.5	0.0242	Sy1.5	2.04	0.77	21.48	O	10 (1.3)	<16.1	K06
IGR J1248.2-5828	12 47 57.84	-58 30 00.2	0.028	Sy1.9	1.02	0.40	22.30				
NGC 4748	12 52 12.40	-13 24 53.0	0.0146	NLSy1	1.27	0.34	20.56	O	3	<0.4	MCP
ESO 323-32	12 53 20.19	-41 38 07.5	0.016	Sy2	1.81	0.40	25.00	O	13 (1.3)	<0.1	K06
3C 279	12 56 11.17	-05 47 21.5	0.5362	QSO/bl	2.15	0.60	20.35				
Mrk 783	13 02 58.84	+16 24 27.5	0.0672	NLSy1	2.21	0.65	21.18	O	2	<5.7	T11
IGR J13038+5348	13 03 59.43	+53 47 30.1	0.03	Sy1.2	2.74	1.59	20.22	O	4	<2.3	MCP
NGC 4941	13 04 13.08	-05 33 05.7	0.0037	Sy2	1.10	0.07	23.64	O	9	<0.1	MCP
IGR J13042-1020	13 04 14.38	-10 20 22.6	0.0104	Sy2	1.42	0.33	25.00	O	4	<0.3	MCP
NGC 4945	13 05 27.28	-49 28 04.4	0.0019	Sy2	25.60	0.54	24.72	M(D?,f)		205.5	B09
ESO 323-77	13 06 26.14	-40 24 52.2	0.015	Sy1.2	2.64	0.77	21.54	O	8	<1.1	MCP
IGR J13091+1137	13 09 05.65	+11 38 01.8	0.0291	XBONG	3.81	0.21	23.63	O	8	<4.3	this work
IGR J13107-5626	13 10 37.0	-56 26 55	-	AGN/RG	1.02	1.10	23.59				
IGR J13109-5552	13 10 43.35	-55 52 11.4	0.104	Sy1	2.43	0.49	<21.66				
IGR J13133-1109	13 13 05.8	-11 07 42	0.03427	Sy1	1.34	8.0	20.42	O	15 (1.3)	<48.3	K06
IGR J13149+4422	13 15 17.25	+44 24 25.9	0.0353	Sy2, L	2.15	0.75	22.72	O	4	<3.2	MCP
IGR J13168-7157	13 16 54.24	-71 55 27.0	0.0705	Sy1.5	1.08	0.38	21.21				
IGR J13187+0322	13 18 31.24	+03 19 48.9	0.606	QSO/bl?	>1.06	0.015	20.28				
NGC 5100	13 20 58.6	+08 58 55	0.03190	L	1.38	4.35	23.16				
MCG-03-34-063	13 22 19.06	-16 42 29.6	0.0213	Sy2	2.34	0.21	23.59	O	37 (0.66)	<23.4	B96
Cen A	13 25 27.61	-43 01 08.8	0.0018	Sy2	62.10	21.20	23.17	M(I?,g)		1.0±0.1	O13
3C287.1	13 32 53.27	+02 00 45.7	0.2156	Sy1	<2.17	0.28	21.21				
ESO 383-18	13 33 26.30	-34 00 58.7	0.0124	Sy2	<0.76	0.52	23.29	O	14 (1.3)	<5.9	K06
MCG-06-30-015	13 35 53.80	-34 17 43.8	0.0077	Sy1.2	4.14	3.64	22.17	O	7	<0.3	this work
NGC 5252	13 38 16.00	+04 32 32.5	0.0230	Sy1.9	4.76	3.00	22.83	O	2	<0.7	MCP
IGR J13415+3033	13 41 11.17	+30 22 41.1	0.0398	Sy2	1.85	0.25	23.47	O	10	<10.0	MCP
SWIFT J1344.7+1934	13 44 15.6	+19 34 00	0.02706	Sy2/L	1.90	0.44	23.39	O	7	<3.2	MCP
IGR J13466+1921	13 46 28.46	+19 22 43.2	0.085	Sy1.2	2.07	0.32	20.27				
Cen B	13 46 49.04	-60 24 29.3	0.0129	RG/type2	1.13	0.49	22.11				
4U 1344-60	13 47 36.00	-60 37 03.8	0.013	Sy1.5	7.23	3.57	23.67				
IGR J13477-4210	13 48 15.2	-42 10 20	0.03860	Sy2	<0.83	1.19	22.80				
IC 4329A	13 49 19.29	-30 18 34.4	0.0160	Sy1.2	20.90	10.40	21.54	O	28	<4.5	this work
LAXG J135417-3746	13 54 16.10	-37 46 43.0	0.0509	Sy1.9	1.42	0.34	22.80				
IGR J13550-7218	13 55 11.45	-72 18 51.3	0.071	Sy2	1.49	0.22	23.28				
PKS 1355-416	13 59 00.2	-41 52 53	0.31300	Sy1	0.75	1.16	21.43				
IGR J14080-3023	14 08 06.57	-30 23 52.6	0.0237	Sy1.5	1.89	0.64	20.56	O	25 (1.3)	<38.5	K06
SWIFT J1410.9-4229	14 10 44.8	-42 28 33	0.03394	Sy2	1.02	2.07	22.76				
Circinus Galaxy	14 13 08.90	-65 20 27.0	0.0014	Sy2	20.20	1.00	24.60	M(D+O,h)		44.9	B09
NGC 5506	14 13 14.87	-03 12 27.0	0.0062	Sy2	14.90	8.38	22.53	M(J/O,e)		28±11	T11
IGR J14175-4641	14 17 03.94	-46 41 39.1	0.076	Sy2	1.62	0.095	23.88				
SWIFT J1417.7+2539	14 17 56.7	+25 43 26	0.23700	BL Lac	2.17	12.0	20.19				
NGC 5548	14 17 59.51	+25 08 12.5	0.0172	Sy1.5	3.00	5.30	20.19	O	5	<0.9	MCP
ESO 511-G030	14 19 22.44	-26 38 40.8	0.0224	Sy1	3.42	1.30	20.70				
H 1419+480	14 21 29.25	+47 47 21.4	0.0723	Sy1.5	<1.76	0.70	20.83				

Table A.1: continue

Name	RA	Dec	z	Class	$F_{\text{H}\alpha}^*$	F_X	Log N_{H}	Notes	Rms*	$L_{\text{H}_2\text{O}}^{**}$	Ref.***
H 1426+428	14 28 32.57	+42 40 24.8	0.1291	BL Lac	1.79	3.38	21.01				
IGR J14301-4158	14 30 12.17	-41 58 31.4	0.0039	Sy2	0.92	0.27	22.08				
NGC 5643	14 32 40.70	-44 10 28.0	0.0040	Sy2	1.10	0.084	23.85	M(?)		13±5	MCP
NGC 5674	14 33 52.2	+05 27 30	0.02493	Sy1.9	1.81	4.85	23.05	O	4	<1.6	MCP
SWIFT J1436.8-1615	14 36 49.6	-16 13 41	0.14454	Sy1/QSO	2.00	7.19	20.88				
NGC 5728	14 42 23.90	-17 15 11.0	0.0093	Sy2	5.38	0.15	24.14	M(D,c)		100±15	MCP
IGR J14471-6414	14 46 28.26	-64 16 24.3	0.053	Sy1.2	1.11	0.48	21.60				
IGR J14471-6319	14 47 14.88	-63 17 19.2	0.038	Sy2	1.36	0.39	22.39				
IGR J14488-4008	14 48 51.0	-40 08 46	0.12300	Sy1.2	0.75	5.27	22.89				
IGR J14492-5535	14 49 17.3	-55 35 45	-	AGN	1.81	3.10	23.08				
IGR J14515-5542	14 51 33.13	-55 40 38.4	0.018	Sy2	2.08	0.53	21.52				
PKS 1451-375	14 54 27.4	-37 47 33	0.31405	Sy1.2	0.98	3.18	20.80				
IGR J14552-5133	14 55 17.80	-51 34 17.0	0.016	NLSy1	1.45	0.96	21.53				
IGR J14561-3738	14 56 08.43	-37 38 52.4	0.024	Sy2	1.55	0.002	>24				
IC 4518A	14 57 41.16	-43 07 55.2	0.0163	Sy2	2.08	0.29	23.15	O	9	<1.5	this work
IRXS J150101.7+223812	15 01 01.8	+22 38 06	0.23500	BL Lac	3.69	0.70	20.54				
MKN 841	15 04 01.20	+10 26 16.1	0.0364	Sy1.5	<3.40	1.62	20.84	O	4	<3.4	MCP
SWIFT J1508.6-4953	15 08 39.0	-49 53 02	-	bl	0.96	2.80	21.31				
IRAS 15091-2107	15 11 59.80	-21 19 02.0	0.0446	NLSy1	2.44	0.90	21.15	O	2	<3.0	T11
PKS 1510-089	15 12 50.5	-09 06 00	0.36000	QSO/bl	3.85	6.31	20.84				
SWIFT J1513.8-8125	15 14 41.92	-81 23 38.9	0.06836	Sy1.2	1.83	1.11	21.88				
ESO 328-36	15 14 47.2	-40 21 35	0.02370	Sy1.8	0.85	7.13	20.84	O	11 (1.3)	<16.9	K06
IGR J15161-3827	15 15 59.70	-38 25 46.8	0.0365	Sy2	<6.22	0.12	22.00				
IGR J15301-3840	15 30 08.0	-38 39 07	0.01553	Sy2	0.77	3.34	22.36				
IGR J15311-3737	15 30 51.79	-37 34 57.3	0.127	Sy1	0.89	1.86	21.32				
MCG-01-40-001	15 33 20.7	-08 42 02	0.02271	Sy2	1.77	4.27	22.59	O	13 (1.3)	<18.4	K06
IGR J15359-5750	15 36 02.8	-57 48 53	-	AGN	2.06	4.97	23.30				
IGR J15415-5029	15 41 26.4	-50 28 23	0.03200	Sy2?	1.04	0.54	<22.04				
NGC 5995	15 48 24.95	-13 45 28.0	0.0252	Sy1.9	3.47	2.20	21.93	O	5	<2.0	MCP
IGR J15539-6142	15 53 35.28	-61 40 58.4	0.015	Sy2	1.58	0.073	23.24				
IGR J15549-3740	15 54 46.76	-37 38 19.1	0.019	Sy2	1.72	0.34	22.76				
IGR J16024-6107	16 01 48.23	-61 08 54.7	0.011	Sy2	0.92	0.30	21.40				
IGR J16056-6110	16 05 51.17	-61 11 44.0	0.052	Sy1.5	1.30	0.14	21.31				
IGR J16058-7253 (1)	16 06 06.9	-72 52 42	0.09000	Sy2	0.90	3.18	23.58				
IGR J16058-7253 (2)	16 05 23.2	-72 53 56	0.06900	Sy2?	0.60	3.50	23.24				
IGR J16119-6036	16 11 51.36	-60 37 53.1	0.016	Sy1.5	2.53	0.33	21.36				
IGR J16185-5928	16 18 36.44	-59 27 17.4	0.035	NLSy1	1.55	0.27	23.02				
Mk 1498	16 28 04.0	+51 46 31	0.05470	Sy1.9	5.09	9.00	23.76	M(J/O?,i)		20±10	MCP
SWIFT J1630.5+3925	16 30 32.6	+39 23 03	0.03056	Sy2	1.59	1.25	23.60	O	13 (1.3)	<3.0	K06
IGR J16351-5806	16 35 13.17	-58 04 49.7	0.0091	Sy2	1.96	0.031	24.68				
IGR J16385-2057	16 38 30.91	-20 55 24.6	0.0269	NLSy1	1.27	0.53	21.08	M(J/O?,f)		12±2	this work****
IGR J16426+6536	16 43 04.07	+65 32 50.9	0.323	NLSy1	3.45	0.0085	20.41				
IGR J16482-3036	16 48 15.20	-30 35 03.7	0.0313	Sy1	<3.85	2.00	21.00	O	34	<21.1	this work
SWIFT J1650.5+0434	16 50 42.70	+04 36 18.0	0.0321	Sy2	2.19	0.32	22.68				

Table A.1: continue

Name	RA	Dec	z	Class	F _{HX} [†]	F _Y [†]	Log N _H	Notes	Rms*	L _{HPO} ^{**}	Ref. ^{***}
NGC 6221	16 52 46.32	-59 13 00.8	0.005	Sy2	1.06	1.41	22.04	O	11 (1.3)	<0.8	K06
ESO 138-1	16 51 20.21	-59 14 04.2	0.0091	Sy2	1.06	0.180	24.18	O	13 (1.3)	<3.0	K06
NGC 6240	16 52 58.97	+02 24 01.7	0.0245	Sy2/L	5.42	0.20	24.30	M(D?,j)		40±20	MCP
Mrk 501	16 53 52.22	+39 45 36.6	0.0337	BL Lac	4.32	16.7	20.07	O	4	<2.9	MCP
IGR J16558-5203	16 56 05.62	-52 03 40.9	0.054	Sy1.2	2.89	1.75	23.27				
SWIFT J1656.3-3302	16 56 16.85	-33 02 11.1	2.4	QSO/bl	3.04	0.44	21.34				
IGR J17009+3559	17 00 53.00	+35 59 56.2	0.113	XBONG	2.13	0.11	23.7				
IGR J17036+3734	17 03 20.20	+37 37 24.9	0.065	Sy1	2.01	0.21	20.39				
IGR J17111+3910	17 11 05.3	+39 08 49	-	AGN	0.96	1.47	20.55				
NGC 6300	17 16 59.47	-62 49 14.0	0.0037	Sy2	6.51	0.86	23.38	M(?)		3.5	B09
MCG+08-31-041	17 19 14.45	+48 58 49.6	0.0242	Sy1/L	7.66	1.10	21.22	O	4	<1.5	MCP
IGR J17204-3554	17 20 21.6	-35 54 32	-	AGN	1.15	2.50	23.20				
Mrk 506	17 22 39.9	+30 52 53	0.04303	Sy1.5	1.81	6.30	<20.70	O	3	<3.5	MCP
SWIFT J1723.5+3630	17 23 23.2	+36 30 10	0.04000	Sy1.5	1.79	8.39	21.28	O	4	<4.0	MCP
PKS 1730-13	17 33 02.7	-13 04 50	0.90200	QSO/bl	1.30	1.46	21.94				
IGR J17348-2045	17 34 59.1	-20 45 34	0.044	Sy2	1.7	2.2	23.23				
GRS 1734-294	17 37 28.35	-29 08 02.5	0.0214	Sy1	8.25	3.84	21.32	O	8	<2.3	this work
IGR J17379-5957	17 37 39.1	-59 56 27	0.01702	Sy2	1.17	6.02	20.79	O	17 (1.3)	<13.5	K06
2E 1739.1-1210	17 41 55.25	-12 11 56.6	0.037	Sy1.2	2.89	1.29	21.18	O	10	<8.7	this work
PKS 1741-03	17 43 58.8	-03 50 05	1.05400	QSO/bl	0.70	2.09	21.27				
IGR J17448-3232	17 44 55.0	-32 32 00	0.05500	Cluster/bl	1.11	1.65	22.40				
IGR J17488-2338	17 48 39.0	-23 35 21	0.24000	Sy1.5	1.58	2.0	22.06				
IGR J17476-2253	17 47 29.71	-22 52 44.3	0.0463	Sy1	1.81	0.26	21.48				
IGR J17488-3253	17 48 55.13	-32 54 52.1	0.02	Sy1	3.96	1.40	21.53	O	9	<2.3	this work
IGR J17513-2011	17 51 13.62	-20 12 14.6	0.047	Sy1.9	2.43	0.58	21.82	O	12	<16.8	this work
IGR J17520-6018	17 51 55.8	-60 19 43	0.11200	Sy2	2.19	2.55	23.11				
IRXS J175252.0-053210	17 52 52.00	-05 32 10.0	0.136	Sy1.2	1.00	0.26	21.33				
NGC 6552	18 00 07.2	+66 36 54	0.02649	Sy2	0.85	0.43	23.85	O	13 (1.3)	<25.0	K06
IGR J18027-1455	18 02 47.37	-14 54 54.8	0.035	Sy1	3.85	0.66	21.48	O	5	<3.9	this work
IGR J18078+1123	18 07 49.9	+11 20 49	0.07800	Sy1.2	1.26	6.32	22.25				
IGR J18129-0649	18 12 50.9	-06 48 24	0.77500	Sy1/QSO	0.66	2.74	21.54				
SWIFT J1821.6+5953	18 21 26.8	+59 55 21	0.0990	Sy2	1.41	1.49	22.88				
IGR J18218+6421	18 21 57.24	+64 20 36.2	0.297	Sy1.2	1.73	1.24	20.54				
IGR J18244-5622	18 24 19.39	-56 22 09.1	0.0169	Sy2	2.66	0.67	23.15				
IGR J18249-3243	18 24 55.92	-32 42 57.7	0.355	Sy1/QSO	1.02	0.52	21.14				
IGR J18259-0706	18 25 57.58	-07 10 22.8	0.037	Sy1	1.36	0.54	21.91	O	5	<4.3	this work
IGR J18308+0928	18 30 50.6	+09 28 42	0.01900	Sy2	1.32	1.30	23.08				
IGR J18311-3337	18 31 14.75	-33 36 08.5	0.0687	Sy2	1.66	0.026	22.15				
PKS 1830-211	18 33 39.92	-21 03 39.9	2.507	QSO/bl	4.83	1.00	22.00				
3C382	18 35 03.39	+32 41 46.8	0.0579	Sy1	5.91	5.98	20.79	O	3	<6.4	MCP
Fairall 49	18 36 58.3	-59 24 09	0.02002	Sy2	1.51	12.0	22.09	O	11 (1.3)	<12.1	K06
ESO 103-35	18 38 20.30	-65 25 41.0	0.0133	Sy2	8.15	2.40	23.27	M(?)		460.5	B09
3C 390.3	18 42 08.99	+79 46 17.1	0.0561	Sy1.5	6.13	2.14	20.63	O	4	<8.0	this work
ESO 140-43	18 44 54.01	-62 21 53.2	0.0142	Sy1.5	3.93	9.50	23.04	O	72 (0.84)	<25.7	B96

Table A.1.: continue

Name	RA	Dec	z	Class	F_{HX}^{\dagger}	F_{X}^{\ddagger}	$\text{Log } N_{\text{H}}$	Notes	Rms*	$L_{\text{H}_2\text{O}}^{**}$	Ref.***
SWIFT J1845.4+7211	18 45 26.2	+72 11 02	0.04630	Sy2	1.00	4.22	22.51	O	2	<2.7	MCP
IGR J18470-7831	18 47 02.83	-78 31 49.5	0.0743	Sy1	1.83	0.80	20.08	O	50 (0.84)	<489.1	G02
PBC J1850.7-1658	18 50 51.6	-16 55 58	-	AGN/RG	1.28	2.19	22.17				
IGR J18538-0102	18 53 48.4	-01 02 30	0.14500	Sy1	1.02	4.0	21.61	O	16 (1.3)	<37.4	K06
ESO 25-2	18 54 40.39	-78 53 54.4	0.0292	Sy1	2.15	0.20	20.92	O			
2E 1853.7+1534	18 56 00.00	+15 38 13.0	0.084	Sy1	2.36	1.22	21.59	O	3	<13.4	this work
2E 1849.2-7832	18 57 07.68	-78 28 21.3	0.0420	Sy1	3.27	0.77	20.92	O	20 (1.3)	<96.7	K06
IGR J19077-3925	19 07 50.36	-39 23 31.9	0.076	Sy1.9	1.49	0.36	21.15				
IGR J19118-1707	19 11 42.64	-17 10 05.1	0.0234	L	<1.17	0.14	23.02				
PKS 1916-300	19 19 28.01	-29 58 09.7	0.1668	Sy1.5-1.8	<1.23	0.62	20.90				
ESO 141-G055	19 21 14.13	-58 40 13.3	0.0371	Sy1.2	4.65	2.45	20.68				
IRXS J192450.8-291437	19 24 51.06	-29 14 30.1	0.352	BL Lac	1.43	0.81	20.86				
SWIFT J1930.5+3414	19 30 13.81	+34 10 49.8	0.0629	Sy1.5-1.8	1.73	0.22	23.44				
SWIFT J1933.9+3258	19 33 47.1	+32 54 26	0.0565	Sy1.2	1.30	13.8	<20.6				
QSO B1933-400	19 37 16.22	-39 58 01.5	0.9655	QSO/bl	1.32	0.19	21.11				
IGR J19378-0617	19 37 33.00	-06 13 05.0	0.0106	NLSy1	1.83	2.70	23.50	O	5	<0.4	this work
IGR J19405-3016	19 40 15.07	-30 15 52.2	0.052	Sy1.2	<1.47	0.11	20.96				
NGC 6814	19 42 40.40	-10 19 24.0	0.0052	Sy1.5	5.66	0.17	21.10	O	8	<0.1	MCP
IGR J19443+2117	19 43 56.2	+21 18 23	-	BL Lac?	1.00	18.3	21.73				
XSS J19459+4508	19 47 32.88	+44 52 58.8	0.0539	Sy2	1.98	0.41	23.04	O	4	<7.4	MCP
IGR J19491-1035	19 49 08.69	-10 34 34.5	0.0246	Sy1.2	1.33	0.56	22.26				
3C 403	19 52 15.82	+02 30 24.3	0.059	Sy2	2.02	1.30	23.60	M(J,a)		1426±174	T03
Cyg A	19 59 28.36	+40 44 02.1	0.0561	Sy2	8.34	1.20	23.30	O	6	<11.9	MCP
1ES 1959+650	19 59 59.8	+65 08 55	0.04700	BL Lac	1.57	91.7	20.85				
ESO 399-20	20 06 57.95	-34 32 54.6	0.0249	NLSy1	1.75	0.13	20.85				
NGC 6860	20 08 46.90	-61 06 01.0	0.01488	Sy1.5	3.90	1.80	21.00	O	78 (0.84)	<30.6	B96
IGR J20159+3713	20 15 28.8	+37 11 00	0.857	QSO/bl	1.11	2-5 (var)	21.89				
SWIFT J2018.4-5539	20 18 01.3	-55 39 31	0.06063	Sy2	3.64	4.01	23.50				
IGR J20186+4043	20 18 38.71	+40 41 00.3	0.0144	Sy2	2.30	0.28	22.76	O	4	<0.5	this work
IGR J20216+4359	20 21 49.04	+44 00 39.4	0.017	Sy2	1.32	0.56	23.11				
IGR J20286+2544(1)	20 28 35.10	+25 43 59.5	0.0139	Sy2/SB	3.34	2.11	23.78	O	4	<0.5	MCP
IGR J20286+2544(2)	20 28 28.90	+25 43 24.6	0.0144	XBONG	1.28	<1.6	23.97	O	33 (1.6)	<23.1	H84
NGC 6926	20 33 06.1	-02 01 39	0.01961	Sy2	1.36	0.07	24.00	M(D?,k)		410±80	MCP
4C +21.55	20 33 32.0	+21 46 22	0.17350	Sy1	2.91	14.0	21.78				
4C 74.26	20 42 37.18	+75 08 02.5	0.104	Sy1	4.27	2.53	21.15	O	4	<27.4	this work
SWIFT J2044.0+2832	20 44 04.00	+28 33 03.0	0.05	Sy1	2.62	0.71	21.24				
Mrk 509	20 44 09.77	-10 43 24.4	0.0344	Sy1.5	7.63	3.4	20.63	O	3	<2.2	MCP
IGR J20450+7530	20 44 34.49	+75 31 58.9	0.095	Sy1	<3.57	0.032	20.30				
S52116+81	21 14 00.00	+82 04 47.0	0.084	Sy1	<2.76	1.21	21.38	O	3	<13.4	this work
IGR J21178+5139	21 17 47.2	+51 38 54	-	AGN	1.81	2.1	22.32				
IRXS J211928.4+333259	21 19 29.13	+33 32 57.0	0.051	Sy1.5	1.55	0.59	21.52				
IGR J21247+5058	21 24 39.33	+50 58 26.0	0.020	Sy1	12.60	4.88	22.89	O	19	<4.8	this work
SWIFT J2127.4+5654	21 27 45.58	+56 56 35.6	0.0147	NLSy1	3.14	4.2	21.90	O	3	<0.4	MCP
CTS 109	21 32 02.1	-33 42 54	0.02997	Sy1.2	1.98	7.6	20.55				

Table A.1.: continue

Name	RA	Dec	z	Class	$F_{\text{H}\alpha}^{\dagger}$	F_{X}^{\dagger}	$\text{Log } N_{\text{H}}$	Notes	Rms*	$L_{\text{H}_2\text{O}}^{**}$	Ref.***
RX J2135.9+4728	21 35 54.2	+47 28 22.3	0.025	Sy1	1.79	0.62	20.30	O	3	<1.2	this work
1RXS J213944.3+595016	21 39 45.10	+59 50 14.0	0.114	Sy1.5	1.02	0.59	21.54				
PKS 2149-306	21 51 55.52	-30 27 53.7	2.345	QSO/bl	2.51	0.80	20.34				
IGR J21565+5948	21 56 04.20	+59 56 04.5	0.208	Sy1	0.98	0.12	21.81				
SWIFT J2156.2+1724	21 56 15.2	+17 22 53	0.03400	Sy1.8	2.00	1.77	23.33				
Mk 520	22 00 41.37	+10 33 08.7	0.0266	Sy1.9	4.13	0.63	22.38	O	2	<0.9	MCP
NGC 7172	22 02 01.90	-31 52 11.6	0.0087	Sy2	7.93	4.30	22.86	O	7	<0.3	MCP
BL Lac	22 02 43.29	+42 16 40.0	0.686	BL Lac	2.40	2.02	21.44	O	8	<2382.3	this work
UGC 12040	22 27 05.8	+36 21 42	0.02133	Sy1.9	2.62	0.86	<22.9	O	5	<1.4	MCP
IGR J22292+6647	22 29 13.84	+66 46 51.5	0.112	Sy1.5	1.11	0.69	21.68				
NGC 7314	22 35 46.23	-26 03 00.9	0.0048	Sy1.9	3.02	1.91	22.02	O	5	<0.1	MCP
IGR J22367-1231	22 36 46.49	-12 32 42.6	0.0241	Sy1.9	2.76	1.09	23.35	O	4	<1.5	MCP
3C 452	22 45 49.10	+39 41 15.0	0.0811	Sy2	3.00	0.50	23.77	O	2	<8.3	MCP
IGR J22517+2218	22 51 53.50	+22 17 37.3	3.668	QSO/bl	3.15	0.26	22.48				
3C 454.3	22 53 57.75	+16 08 53.6	0.859	QSO/bl	19.17	6.10	21.28				
QSO B2251-178	22 54 05.88	-17 34 55.3	0.0640	Sy1.2	6.66	2.00	22.33	O	4	<10.4	this work
KAZ 320	22 59 32.9	+24 55 06	0.03450	NLSy1	1.49	10.1	20.68				
NGC 7465	23 02 00.95	+15 57 53.6	0.0066	Sy2/L	2.62	0.41	23.66	O	3	<0.1	MCP
NGC 7469	23 03 15.75	+08 52 25.9	0.0163	Sy1.5	4.49	2.30	20.46	O	6	<1.0	MCP
MCG-02-58-022	23 04 43.48	-08 41 08.6	0.0469	Sy1.5	4.30	3.18	20.56	O	3	<4.2	this work
NGC 7479	23 04 56.6	+12 19 22	0.00794	Sy1.9	1.40	0.33	24.30	M(D?,1)		12±8	MCP
NGC 7582	23 18 23.49	-42 22 14.1	0.0052	Sy2	<2.80	0.23	24.04	O	10	<0.2	MCP
IGR J23206+6431	23 20 36.58	+64 30 45.2	0.0717	Sy1	<0.66	0.55	21.95				
RHS 61	23 25 54.2	+21 53 14	0.12000	Sy1	1.43	4.32	20.59				
PKS 2325+093	23 27 33.6	+09 40 09	1.84300	QSO/bl	2.45	2.9	20.60				
IGR J23308+7120	23 30 37.68	+71 22 46.6	0.037	Sy2?	<0.53	0.14	22.96	O	2	<1.7	this work
IGR J23524+5842	23 52 22.11	+58 45 30.7	0.164	Sy2?	1.23	0.28	22.46	O	3	<51.1	this work
IGR J23558-1047	23 55 59.3	-10 46 45	1.10800	Sy1/QSO	5.26	0.08					

Sources in boldface belong to the complete AGN catalog reported in Malizia et al. (2009). The format on the relevant digits in the coordinates are those originally reported (Malizia et al. 2012, 2016). Maser types: D=disc; J=jet; O=outflow; /=or; +=plus. For possible limits on this classification see Sect. 6. References for the Maser type: a) MCP at <https://safe.nrao.edu/wiki/bin/view/Main/PublicWaterMaserList> (web page updated at November 10, 2018); b) Henkel et al. (2005); c) Kamali et al. (2017); d) Kondratko et al. (2005); e) Tarchi et al. (2011); f) Humphreys et al. (2016); g) Ott et al. (2013); h) Greenhill et al. (2003); i) Greenhill et al. (2009); j) Hagiwara & Edwards (2015); k) Sato et al. (2005); l) Wang et al. (2010). † 2–10 keV and 20–100 keV flux in units of 10^{-11} erg cm^{-2} s^{-1} . * 1σ rms in mJy, calculated over a 0.3 km s^{-1} wide channel, unless otherwise specified (different channel widths are reported in brackets); ** Water maser isotropic luminosities are in unit of L_{\odot} , where $L_{\odot} = 3.826 \cdot 10^{33}$ erg s^{-1} . We calculate the upper limits for the undetected sources using the formula: $L_{\text{H}_2\text{O}}[\text{L}_{\odot}] = 0.023 \times S[\text{Jy}] \times \Delta v[\text{km s}^{-1}] \times D^2[\text{Mpc}^2]$, where $S[\text{Jy}]$ and $\Delta v[\text{km s}^{-1}]$, are the 5σ rms and the channel spacing, respectively; D is the distance in Mpc, derived using the redshift in column 4 and $H_0 = 70 \text{ km s}^{-1} \text{ Mpc}^{-1}$. *** References for the rms (undetected sources) or the isotropic maser luminosity (detected sources): B96: Braatz et al. (1996); B09: Bennert et al. (2009) and references therein; G96: Gallimore et al. (1996); G02: Greenhill et al. (2002); H84: Henkel et al. (1984); K05: Kamenno et al. (2005); K06: Kondratko et al. (2006); MCP: Megamaser Cosmology Project webpage (<https://safe.nrao.edu/wiki/bin/view/Main/MegamaserCosmologyProject>); O13: Ott et al. (2013); P03: Peck et al. (2003); P15: Pesce et al. (2015); T03: Tarchi et al. (2003); T11: Tarchi et al. (2011). **** The maser in IGRJ16385-2057 was detected during our survey (Sect. 3.3), a detailed analysis have been reported in Tarchi et al. (2011).

Appendix B: Maser types

Of the INTEGRAL AGN with maser detection, only six sources (IGR J05081+1722, NGC 3081, NGC 3783, NGC 5643, NGC 6300, and ESO 103-G35) so far have no associated maser type. Here we discuss each source individually and provide some clues on their most likely maser type.

IGR J05081+1722 is interesting from many points of view. It belongs to an IR-luminous interacting pair of galaxies that is characterised by a luminosity for the whole system (made of a combination of star formation and accretion) of $\log(L_{IR}/L_{\odot})=11.2$. The system is at an early stage of merger (11.3 kpc distance) and is known to host an AGN that has optically been classified as Seyfert 2 plus a normal galaxy. The AGN, which is also the component in the system that displays water maser emission, hosts a molecular outflow and probably also a disc wind (Yamashita et al. 2017; Ballo et al. 2015). NGC 3783 is one of the most intensively monitored Seyfert galaxy at high energies. It is known to exhibit UV absorbers plus a series of ionised X-ray absorbers that are variable in time (Fukumura et al. 2018; Mehdipour et al. 2017). These have generally been interpreted as associated with a strong obscuring outflow in the nuclear region. In contrast to other sources in our sample, neither IGR J05081+1722 nor NGC 3783 display strong X-ray absorption (their column densities are about 10^{22} at cm^{-2}), suggesting that their water maser emission might indeed be associated with a jet or outflow. Because no clear jet emission appears to be present in NGC 3783, but only a diffuse radio emission on tens of pc-scales (Oriente, & Prieto 2010), the outflow remains the only option; the situation is less clear in IGR J05081+1722, but the outflow is a viable possibility to explain water maser emission in this source as well.

Single-dish maser spectra for these sources⁵ are consistent with an outflow origin. In particular, the maser emission in IGR J05081+1722 is blueshifted with respect to the systemic velocity (by about 100 km/s) and appears to consist of a handful of narrow components that are attached to a broader feature. The maser spectrum in NGC 3783 is instead characterised by a group of narrow features that are close to the systemic velocity of the galaxy. Clearly, the nature of the maser cannot be uniquely assessed without high-resolution follow-up studies.

NGC 6300 and ESO 103-G35 are type 2 mildly absorbed AGN with column densities of about 10^{23} at cm^{-2} . NGC 6300 features a slightly resolved radio core at arcsecond resolution with an extension in the southern direction (Morganti et al. 1999), and there is also evidence for a complex molecular hydrogen structure made of an edge-on outflow superimposed on a rotating disc (Davies et al. 2014). ESO 103-G35 does not show evidence for a radio jet; furthermore, an in-depth analysis of the galaxy optical properties brought no clues on the origin of water maser emission, including no evidence for outflows (Bennert et al. 2004). Despite this, the source has been reported in X-rays as the site of a highly ionized outflow (Gofford et al. 2015). As in the two previous cases, the interpretation (among others) of an outflow origin of the water maser emission does not contradict the shape of the maser spectra⁶ for NGC 6300 (Greenhill et al. 2003) and ESO 103-G35. In both cases, emission is detected close to (or slightly redshifted with respect to) the systemic velocity of the target, and it is comprised of a very small number of narrow features (one in the case of ESO 103-G35) that are placed above a broader component. A somewhat different spectrum of ESO 103-G35 is shown in the detection paper (Braatz et

al. 1996), however, where emission from a single 20-km/s wide line is shown that is clearly redshifted by ~ 100 km/s with respect to the systemic velocity.

Finally, NGC 5643 and NGC 3081 are heavily absorbed objects (NGC 3081 is also Compton thick). In these objects, nuclear discs are likely to be the site where maser emission develops. Recent observations with ALMA of NGC 5643 (Alonso-Herrero et al. 2018) have at the parsec scale resolved a massive rotating disc or torus of molecular gas with strong non-nuclear motion features associated with radial outflow in the disc. Interestingly, the maser emission appears to be centrally located with respect to the inner (nuclear) part of this structure, which is also tilted with respect to the larger scale disc. The inner structure of NGC 3081 has instead been mapped with the Gemini Multi Object Spectrograph (GMOS-IFU) (Schnorr-Müller et al. 2016) and was found to host an even more complex structure, but at the kilo-parsec scale: this includes rotation in the galaxy disc plane, a bipolar outflow from the AGN, non-circular motions along the nuclear bar, and an interaction between the bipolar outflow and the disc gas. Both objects thus resemble the well-known maser sources NGC 1068 and the Circinus galaxy, where water maser disc emission is coupled to jet or outflow maser radiation. This suggests a similar interpretation for NGC 5643 and NGC 3081 as well. Because the single-dish spectrum alone⁷ has a relatively low signal-to-noise ratio, it is not possible to infer a secure hypothesis on the nature of the maser in NGC 3081. The maser in NGC 5643 (Greenhill et al. 2003, and MCP webpage) instead indicates redshifted (50–100 km/s with respect to the systemic velocity) emission that consists of a relatively broad feature with two or three peaks and might be due to a blending of features. Speculatively, the maser might then either be associated with a jet (a diffuse radio jet on either side of the nucleus is indeed visible in a high-sensitivity image obtained with the Very Large Array, Leipski et al. 2006) or with a rotating structure of which we only see the redshifted lines or the systemic lines when a large uncertainty in the reported target recessional velocity is accounted for.

As mentioned before, however, confident clues on the association of the maser emission with the AGN activity and on the maser nature of all six objects must await follow-up (interferometric) studies. In particular, all these maser sources, with the exception of ESO 103-G35 (~ 460 solar luminosities), have moderate maser isotropic luminosities: the luminosities of four targets are only slightly higher than the paradigmatic threshold that separates kilo- and megamasers (35, 20, 17, and 13 solar luminosities for IGR J05081+1722, NGC 3783, NGC 3081, and NGC 5643, respectively), and one object, NGC 6300 (~ 3.5 solar luminosities), is below that threshold. While this is still consistent with an outflow-related origin of the maser emission (Tarchi et al. 2011 discuss an analogous origin for the water maser detected in a sample of NLSy1 that has similar luminosities to ours), an association with star formation activity for these masers, especially for that in NGC 6300, cannot be ruled out a priori.

⁵ As shown on the MCP webpage

⁶ As shown on the MCP webpage

⁷ Shown on the MCP webpage